

**Customizable Intraoperative Neural Stimulator and Recording
System for Deep Brain Stimulation Research and Surgery**

by

Sunjay Dodani

A dissertation submitted in partial fulfillment
of the requirements for the degree of
Doctor of Philosophy
(Biomedical Engineering)
in the University of Michigan
2013

Doctoral Committee:

Assistant Professor Parag G. Patil, Chair
Professor J. Wayne Aldridge
Professor Michael P. Flynn
Professor Euisik P. Yoon

TABLE OF CONTENTS

LIST OF FIGURES	iv
LIST OF TABLES	vi
Abstract	vii
Chapter 1 : Introduction	1
Aims	1
Background	2
References	5
Chapter 2 : Intra-Operative Data Acquisition System for Deep Brain Surgical Procedures	6
Abstract	6
Introduction	7
Methods	7
Results	12
Conclusions	18
References	20
Chapter 3 : An Automated Targeting System for Subthalamic Nucleus Deep Brain Stimulation	22
Abstract	22
Introduction	24
Methods	25
Results	31
Discussion	33
Conclusion	34
References	35
Chapter 4 : Subthalamic Beta Activity and Optimal Deep Brain Stimulation Sites Spatially Dependent	37
Abstract	37
Introduction	38
Methods	39

Results	42
Discussion	45
References	48
Chapter 5 : Activation of Subthalamic Nucleus in Local Field Potentials and Single Units during Response Inhibition	51
Abstract	51
Introduction	53
Methods	54
Results	58
Discussion	62
References	65
Chapter 6 : Conclusion	67
Appendix	68

LIST OF FIGURES

Figure 2.1: IODA Architecture	11
Figure 2.2: A filtered signal recorded from within the STN of a Parkinson disease patient using IODA	13
Figure 2.3: A spectrogram of 5 Hz to 30 Hz power in the LFP signal recorded from the STN	13
Figure 2.4: The baseline noise for the IODA system	14
Figure 2.5: Medtronic 8840 (Blue plot) vs IODA stimulator (Green plot)	15
Figure 2.6: Examples of IODA custom stimulation profile capability	15
Figure 2.7: Analog data signals from joystick movements and photodiode sensor	16
Figure 2.8: Typical electrophysiological display from MER signals	17
Figure 2.9: IODA's alternate primary electrophysiological view	18
Figure 3.1: Experimental method	25
Figure 3.2: A) Potential trajectories and the associated intensities along each track, B) 3-T MRI coronal view of STN targeted potential voxel trajectories in an 8 voxel search window	28
Figure 3.3: Distribution of potential voxel trajectory scores for an individual MER track	29
Figure 3.4: Scoring Method Simulation	30
Figure 3.5: Correlation of Planned trajectory and Estimated MER trajectory	32
Figure 3.6: Distances from DBS lead in X and Y direction for calculated and plan trajectories	32
Figure 4.1: STN midpoint analysis on a three dimensional STN model	42
Figure 4.2: Trajectories of beta power through the STN	43
Figure 4.3: Correlation plots for optimal contact locations, peak beta power sites, and the DB-STN	44
Figure 4.4: Averaged group for medial and lateral trajectories through the STN	45
Figure 5.1: Stop-signal paradigm used intraoperatively with PD patients	57
Figure 5.2: Race model reaction times for movement trial types	59
Figure 5.3: Normalized z-score plots for triggered events for theta, alpha, and beta bands	60

Figure 5.4: Scalogram plots from 5 Hz to 30 Hz for trial types centered on the Stop-Signal cue 61

Figure 5.5: Average firing rate for the recorded single units across the three trigger events 62

LIST OF TABLES

Table 2.1: The system specifications for IODA	8
Table 5.1: Counts for each trial type, reaction time, and firing rate for each recording session.	59

Abstract

The work presented in this dissertation is of the development and validation of an intraoperative neural stimulator and recording system for use in deep brain stimulation (DBS) surgeries. Intraoperative targeting systems provide neurosurgeons with raw electrophysiological data through microelectrodes used for determining location in the brain. Typical analysis of these signals is subjective and heavily dependent on experience and training. There are significant deficits to the available targeting systems, limiting the use in both clinical and research applications. This intraoperative data acquisition system (IODA) is capable of recording electrophysiological signals in a wideband frequency range. It also has the ability to stimulate with standard and custom stimulation parameters used for targeting and clinical efficacy of DBS on targeted locations in the brain.

The system was validated with three different applications demonstrating the flexibility and necessity of IODA. The first, a clinical application, illustrated the improvement IODA had on the targeting accuracy of DBS leads in the subthalamic nucleus (STN) over current targeting methods. IODA's navigation system showed microelectrode probe locations to be significantly closer to final DBS lead positions, $2.33 \text{ mm} \pm 0.2 \text{ mm}$ $P = .01$, compared to the planned trajectory position, $2.83 \text{ mm} \pm 0.2 \text{ mm}$. IODA was also validated with a clinical science application attempting to resolve a highly contested topic, the location of the most optimal stimulation site for chronic DBS of the STN. Beta oscillations of local field potentials (LFP) recorded through IODA enabled the confirmation of previous findings for optimal sites of stimulation to be both, sites of peak beta activity and the dorsal border of the STN. With IODA's precise targeting, we found sites of optimal stimulation were not different from the dorsal border of the STN when trajectories were lateral of the STN midpoint, $0.35 \pm 1.43 \text{ mm}$, $P = .51$, and were not different from peak beta hypersynchrony when trajectories were medial of the STN midpoint, $-0.36 \pm 1.6 \text{ mm}$, $P = .57$. Finally, we confirmed recent findings of STN involvement in movement inhibition through a basic science application. Through wideband recordings and integrated task tools made with IODA, we corroborated the recent findings

suggesting increased activation in the theta, alpha, and beta bands of the LFP in response to movement and movement inhibition cues. We also confirmed that single unit activity in these recording locations within the STN responded with significant decreases in firing rates in response to inhibition cues, $P < .001$.

Through in depth experimentation using IODA we have validated the utility and adaptability of this system for use within DBS surgeries. There is significant potential for use of IODA outside of DBS in other surgical procedures requiring precise neural targeting. Additionally there are many applications of IODA for use in research for other neurodegenerative disease including Essential Tremor and Depression. The use of this system has enables neurosurgeons to reduce surgical time, risk, and error for DBS procedures and made entry easier for those less experienced in this procedure. The novel system described in this work enables neurosurgeons, electrophysiologists, and researchers to significantly improve clinical efficacy of DBS and the understanding of physiological effects of neurodegenerative diseases.

Chapter 1 : Introduction

In-vivo analysis of a living human brain is a rare opportunity usually only achieved during clinical neurosurgery. Only during selective types of surgery, specifically Deep Brain Stimulation (DBS) surgery, can we attempt to understand the circuitry and function of different brain structures in humans. DBS is the application of voltage or current at set frequencies and amplitude to a specific location in the brain via an implanted electrode. The surgery is currently approved by the FDA for the treatment of Parkinson disease and Essential Tremor as an effective method for the control of primary motor control symptoms of both diseases. Given the nature of DBS, a brief window of access is possible to attain data through probes while the patient is conscious. Intraoperative analysis on living human brains requires sophisticated electronics which can record and stimulate from within the brain. The most sophisticated commercially available systems can only provide limited recording and stimulation capabilities with little flexibility in varying the parameters of each capability. These systems were also designed to assist in clinical assessments of DBS surgeries and were not intended to explore potential improvements to the surgery or assist in answering fundamental questions regarding the brain. We propose to develop an intraoperative data acquisition (IODA) system that can record and stimulate neural tissue with the ability to control the parameters of both to explore the effects of DBS. The system will be applied to specific structures in the brain during DBS surgeries so we can objectively measure the effects of varying DBS parameters on these brain structures. Our goal is to use IODA to investigate improvements in DBS therapy and to explore clinical science research of the brain.

Aims

In order to ensure the functionality and use of this system, we propose three applications of validation: 1) clinical application of the system, 2) clinical science application, and 3) basic science application.

The first application of IODA is to test its functionality as a surgical navigation tool during DBS procedures. We hypothesize that using IODA to collect microelectrode recording data and high resolution imaging data; IODA can provide more precise intraoperative electrode location compared to current methods. Additionally IODA can enable neurosurgeons to reduce surgical operating time, risk, and error.

The second application utilizes the system's wideband recording to investigate optimal stimulation sites within the subthalamic nucleus region for DBS electrodes as they relate to the beta frequency band of local field potentials. This has been a widely contested topic in recent studies and using IODA with high resolution imaging we hypothesize that sites of optimal stimulation and beta hypersynchrony are spatially dependent with respect to the STN.

The third validation application of IODA is to integrate intraoperative patient testing with microelectrode recordings to draw basic science conclusions regarding the nature of the subthalamic nucleus in Parkinson's disease. We hypothesize that recording single unit and local field potential activity from the STN of patients performing a motor movement task, we can confirm recent findings regarding the effects of movement and inhibition to movement in various frequency bands of the STN.

Background

Deep Brain Stimulation

Deep Brain Stimulation is the application of electrical current to structures of the brain through implanted electrodes connected to a pulse generating source. DBS was a major step forward for the treatment of such diseases as Parkinson's and Essential tremor which were previously treated using ablative techniques. DBS offers similar behavioral effects as lesioning with the advantages of being adjustable and reversible.¹ However the full physiologic mechanism underlying the effects of DBS are still not well understood.

DBS surgeries are performed under local anesthetic so patients can remain conscious and alert for stimulation testing to measure symptom improvements. Patients are not sedated because the effects of general anesthesia have been shown to disrupt the firing patterns in the sensory motor network, making intra-operative testing difficult and potentially inconclusive.² Targeting of structures in the brain is done with a combination of technologies and methods. The neurosurgeon uses computer modeling with CT and MRI images to predict an appropriate

trajectory for the implant of the DBS electrode. Using a microelectrode (MER) prior to implanting the DBS electrode, the neurosurgeon and attending electrophysiologist determine locations and structures in the brain by monitoring neural signals recorded from the MER probe through audio and visual displays from the signal.³

Neurodegenerative Diseases

Parkinson's disease (PD) is a debilitating neurodegenerative disorder characterized by motor symptoms including tremor, rigidity, and bradykinesia that affects the basal ganglia. The basal ganglia are a network of nuclei associated with voluntary motor control.⁴ The network is made up of the striatum, global pallidus (GP), thalamus, substantia nigra (SNr), and the STN. The current model for the pathways of the basal ganglia involves a direct and indirect pathway. The direct pathway connects the striatum to the GPi to the motor thalamus. The direct pathway is associated with excitatory dopamine receptors known as D1 receptors. Neurons with D1 receptors project from the striatum to excite an inhibitory output from the GPi to the thalamus. The inhibitory output from the GPi causes a dis-inhibition of motor thalamus firing rate, thus increasing the firing rate of its cells and reducing the inhibition of initiated movement.⁵ The indirect pathway in the basal ganglia is believed to be ultimately regulated by the STN.⁵ The indirect pathway is associated with neurons containing inhibitory dopamine receptors referred to as D2 receptors. Neurons with D2 receptors project from the striatum to the GPe causing a dis-inhibitory output to the STN. The STN is therefore disinhibited and its cells increase firing, leading to the inhibitory activation of the GPi and SNr. Both the GPi and SNr inhibit the thalamus thus reducing the excitatory thalamic input to other motor areas through the motor cortex. The indirect pathway is believed to inhibit unwanted movement.⁵

As Parkinson's disease progresses, motor symptoms worsen and the side effects from medication become more prevalent. PD is thought to affect both the direct and indirect pathway through the depletion of dopamine. The depletion of dopamine in the direct pathway affects D1 receptors which cause the pathway to be underactive, decreasing the firing of the thalamic neurons and inhibiting movement. In the indirect pathway, dopamine depletion affects D2 receptors causing an overactive inhibitory signal in the GPi believed to be responsible for rigidity and akinesia symptoms of PD.⁵ DBS surgery becomes an option for those patients whose quality of life is impacted from the progression of motor symptoms from PD and the side effects

associated with higher doses of PD medication..^{6,7} DBS surgery for PD is typically targeted for the stimulation of the STN, GPi, or the VIM of the thalamus depending on the primary symptom of the individual patient.⁸ However the STN is generally targeted since it has been shown that stimulation in the STN inhibits the overactive inhibitory signal allowing the STN to increase firing of its cells.⁹

Essential Tremor (ET), the most common form of pathologic tremor, is a debilitating neurodegenerative disorder. Similar to PD, ET can be treated with medication for tremor symptoms. However as the disease progresses quality of life is markedly decreased due to side effects from higher doses of medication to control for an increase in symptom intensity. DBS surgery for ET typically targets the VIM of the thalamus for stimulation as it has been shown to control 70% to 90% of tremor in ET patients.^{5, 10}

Significant research has been done in the basal ganglia to better understand the motor pathway. Single unit recordings and Local Field Potentials (LFPs), signals which are the measure of electrical activity from tissue near the recording source, have been used to explain the function and activity of different components in the pathway.

Specifically in the STN, LFP activity has been investigated to understand the effects of stimulation during DBS on the motor pathway.¹¹ Increases in the alpha band of the LFP, 1-7Hz, in the STN during stimulation was shown to correlate with improved symptom response. This responses is in the LFP is believed to be how DBS stimulation helps to normalize STN hyperactivity in patients with PD.¹¹ LFP activity in the STN has also been used to study the characteristics of movement in patients with PD.^{12, 13} Single unit recording has also shown feasible in the STN using microelectrodes (MER). Single unit recordings are essential to determine detail, which cannot be drawn from LFPs, regarding the structure of interest. Single unit data has been used to characterize the role the STN has in patients with Dystonia by measuring the firing rate, bursting, and oscillatory activity.¹

References

1. Schrock LE, Ostrem JL, Turner RS, Shimamoto SA, Starr PA. The subthalamic nucleus in primary dystonia: single-unit discharge characteristics. *J Neurophysiol.* Dec 2009;102(6):3740-3752.
2. Stamatakis EA, Adapa RM, Absalom AR, Menon DK. Changes in resting neural connectivity during propofol sedation. *PLoS One.* 2010;5(12):e14224.
3. Snellings A, Sagher O, Anderson DJ, Aldridge JW. Identification of the subthalamic nucleus in deep brain stimulation surgery with a novel wavelet-derived measure of neural background activity. *J Neurosurg.* Oct 2009;111(4):767-774.
4. McIntyre CC, Savasta M, Walter BL, Vitek JL. How does deep brain stimulation work? Present understanding and future questions. *J Clin Neurophysiol.* Jan-Feb 2004;21(1):40-50.
5. Purves D AG, Fitzpatrick D. *Neuroscience.* 2nd ed: Sinauer Associates; 2001.
6. Lyons MK. Deep brain stimulation: current and future clinical applications. *Mayo Clin Proc.* Jul 2011;86(7):662-672.
7. Mera T, Vitek JL, Alberts JL, Giuffrida JP. Kinematic optimization of deep brain stimulation across multiple motor symptoms in Parkinson's disease. *J Neurosci Methods.* Jun 15 2011;198(2):280-286.
8. Katayama Y. [Deep brain stimulation therapy for involuntary movements]. *Rinsho Shinkeigaku.* Dec 2001;41(12):1079-1080.
9. Filali M, Hutchison WD, Palter VN, Lozano AM, Dostrovsky JO. Stimulation-induced inhibition of neuronal firing in human subthalamic nucleus. *Exp Brain Res.* Jun 2004;156(3):274-281.
10. Schuurman PR, Bosch DA, Bossuyt PM, et al. A comparison of continuous thalamic stimulation and thalamotomy for suppression of severe tremor. *N Engl J Med.* Feb 17 2000;342(7):461-468.
11. Rossi L, Marceglia S, Foffani G, et al. Subthalamic local field potential oscillations during ongoing deep brain stimulation in Parkinson's disease. *Brain Res Bull.* Jul 30 2008;76(5):512-521.
12. Burgess JG, Warwick K, Ruiz V, et al. Identifying tremor-related characteristics of basal ganglia nuclei during movement in the Parkinsonian patient. *Parkinsonism Relat Disord.* Dec 2010;16(10):671-675.
13. Klostermann F, Nikulin VV, Kuhn AA, et al. Task-related differential dynamics of EEG alpha- and beta-band synchronization in cortico-basal motor structures. *Eur J Neurosci.* Mar 2007;25(5):1604-1615.
14. Baudrexel S, Witte T, Seifried C, et al. Resting state fMRI reveals increased subthalamic nucleus-motor cortex connectivity in Parkinson's disease. *Neuroimage.* Apr 15 2011;55(4):1728-1738.
15. Holdefer RN, Cohen BA, Greene KA. Intraoperative local field recording for deep brain stimulation in Parkinson's disease and essential tremor. *Mov Disord.* Oct 15 2010;25(13):2067-2075.
16. Kane A, Hutchison WD, Hodaie M, Lozano AM, Dostrovsky JO. Enhanced synchronization of thalamic theta band local field potentials in patients with essential tremor. *Exp Neurol.* May 2009;217(1):171-176.

Chapter 2 : Intra-Operative Data Acquisition System for Deep Brain Surgical Procedures

Abstract

Objective: Deep brain stimulation (DBS) of the subthalamic nucleus (STN) is an effective therapy for Parkinson's disease (PD). Microelectrode recording (MER) is typically used for intraoperative targeting of the STN. Commercial systems used for intraoperative targeting are limited in functionality and features. The aim of this work is to develop a system capable of providing enhanced clinical and research functionality for users during DBS surgeries.

Method: We developed a targeting system using FDA approved components to record and stimulate neural tissue during DBS. We validated intraoperatively recorded signals with published findings of DBS research and commercially available targeting systems. We also demonstrated the extended capabilities in stimulation profiles, user interface, and integration with DBS research.

Results: We used our intraoperative data acquisition (IODA) system in over 75 DBS surgeries. We validated capabilities for wideband recording, stimulation, and research applications with physiologic and clinical findings. We also validated the use of magnetic resonance imaging (MRI) as a valuable interface for system users.

Conclusion: We present a novel system for use intraoperatively for data acquisition and neural stimulation during DBS procedures. This system is capable of providing necessary information for neurosurgeons and electrophysiologists to perform standard electrophysiological analysis for target localization as well as DBS research.

Clinical Impact: This system can be used for both clinical and research applications during DBS cases. The system can potentially enable neurosurgeons that are not specialty trained to perform DBS and help reduce surgical time and error for experienced users.

Introduction

Deep brain stimulation (DBS) is a well-established surgical therapy for Parkinson's disease [1]. Chronic bilateral high-frequency stimulation of the subthalamic nucleus (STN) alleviates the motor symptoms of Parkinson's disease. Often, intraoperative confirmation of the STN location is performed through microelectrode recording (MER) [2-5]. MER signals enable neurosurgeons and electrophysiologists to determine the location of the MER probe relative to the STN target intraoperatively using traditional electrophysiological analysis [6].

During surgery, MER signals are digitally converted for display and audio analysis using commercially available neuromodulation targeting systems. These systems are designed primarily for experienced clinical users with a technical understanding for neural signal modulations and stimulation. Most available targeting systems are limited in recording frequency range, compatibility with existing DBS equipment, integration of research tasks, and stimulation capabilities. Intraoperative MER analysis uses the high frequency band (HFB), typically 500 Hz to 2 kHz, for STN targeting [6-10]. However, there has been significant research in the local field potential (LFP) signals, typically 1Hz to 250 Hz, role in neurodegenerative diseases [11-18]. The available targeting systems offer the ability to record HFB signals from MER but not LFP, thus limiting the use of these systems in DBS research.

We present an intraoperative data acquisition (IODA) system for targeting and neuromodulation for DBS procedures. The system is capable of both clinical and research tasks because it can record frequencies in a wideband range that includes HFB and LFP signals. IODA also has the ability to replicate standard stimulation profiles used by DBS devices as well as apply custom stimulation profiles for DBS research. The system is able to integrate with existing DBS equipment, accessories, and experimental research tools. Additionally, we have integrated magnetic resonance imaging (MRI) into IODA to create an alternative primary display for a more intuitive use of targeting systems. By providing a simpler and more intuitive interface for IODA, we aim to create a system that can be used by neurosurgeons interested in DBS but are not specialty trained.

Methods

IODA was designed for both intraoperative recording and stimulation of brain tissue. We integrated FDA approved components for signal amplification and electrical stimulation through microelectrodes with custom software. Specifications were determined through physiological requirements for signal recording and analysis as well as user requirements (Table 2.1).

System Specifications

	Required Specification Range	IODA Specification Range
MER Probe Impedance	500 kOhm to 2MOhm	500 kOhm to 2MOhm
System input Impedance	1MOhm	100MOhm
Sampling frequency	>24kHz	1 Hz – 52kHz
Signal Filtering	>300Hz	1Hz – 8kHz
Signal Gain	1 – 100,000	100-1,000,000
High Frequency Band	300Hz – 5kHz	300Hz – 5kHz
LFP	<250Hz	<250Hz
Noise Floor	<10uV	<5uV
Stimulation waveform	Square Wave	Square, triangle, custom
Stimulation frequency	1Hz – 300Hz	1Hz – 300Hz
Stimulation pulse width	10 microSec – 1 sec	10 microSec – 1 sec
Stimulation Amplitude	0V – 10V	0V – 10V, 0mA – 10mA
Graphical User Interface	Raw signal view, Stim, motor, and filter control	Raw signal view, Stim, filter, volume, motor, MRI view, patient tasks, and file writing controls

Table 2.1: The system specifications for IODA and the required specifications based on physiological and user needs.

Microelectrode Recording Probe

The microelectrode recording (MER) probe is used to acquire neural signals during DBS surgery. In our surgical setup, the probe is made of tungsten and stainless steel (microTargeting Electrode, FHC; Bowdoin, ME). The probe tip is 40 micrometers in diameter and the electrode shank is 250 micrometers in diameter. The electrode is configured for differential recording using the probe tip and the reference ring set 1 millimeter apart. The impedance of these MER probes range from 500 kOhms to 2MOhms. A low MER impedance is critical for stimulation in both micro and macro settings. When applying voltage controlled stimulation the current delivered to the intended neural tissue is dependent on the impedance of the electrode it passes through. A high impedance electrode reduces the energy delivered to the neural tissue and thus reduces the observed effect of the intended stimulation.

Wideband Signals

The wideband signal specification we used is based on current signal analysis methods for neural signals. Traditionally, intraoperative electrophysiological signal analysis requires high frequency signals usually between 300 Hz and 5 kHz. This frequency band enables neurosurgeons and electrophysiologists to monitor neuronal background activity and single unit firing changes as the MER probe is advanced in the brain. This range is primarily used to identify DBS targets such as the subthalamic nucleus (STN) for Parkinson's disease and the ventral intermediate nucleus (VIM) of the thalamus for patients with Essential Tremor. These structures have signature firing patterns and are identifiable using classic electrophysiological acoustic analysis.

The local field potential (LFP) signal is generally considered to be useful for understanding integration of various structures and local neuronal activity in recording areas. The LFP is typically considered to range from 1Hz to 250Hz. Within the LFP frequency range there are multiple smaller bands considered to be critical in the communication between different brain structures and regions. Namely, the beta band (13-30Hz) is considered to be of significant importance in the understanding of neurodegenerative diseases such as Parkinson's.

Noise Floor

The noise floor of a targeting system must be low and well controlled in order to maintain a good signal to noise ratio. Noise levels in surgical environments are difficult to control for due to excessive electrical interference from various surgical equipment including electrocardiography (EKG) monitors, intraoperative CT imaging systems, surgical lights, ultrasound systems, and cauterizing equipment. These electrical interferences usually affect and corrupt low frequency signal recording. It is for this reason most commercially available surgical recording platforms only record high frequency signals. Typically, neuronal spikes have amplitudes ranging from 50 μV to 150 μV [6, 8] and LFP signals are on the order of magnitude of 10 μV [15]. A noise floor of at least 10 μV is necessary for capturing LFP activity during DBS surgeries.

Stimulation

The stimulation of neural tissue is the premise for the beneficial effects of DBS. Although there is little evidence for a definitive physiological explanation of high frequency stimulation in the brain, the effects are well documented. The clinical long term stimulation settings for each patient are determined by neurologists, but are bounded by device limitations. Currently, DBS devices have a fixed waveform, square-wave, with variable frequency, pulse width, and amplitude ranges. The waveform can range between 10 Hz to 300 Hz stimulation frequency, 10 μ seconds to 1 second pulse width, and range in amplitude between 0 volts and 10 volts.

Graphical User Interface

The IODA GUI was designed to provide a traditional electrophysiological view of neural signals as well as more intuitive views using MR imaging. Most electrophysiological systems depict raw neural signals recorded from MER probes as the primary view. Typical systems integrate amplifiers, filters, motor controls, volume, and stimulators into the GUI and provide the user control over each of these parameters.

System Architecture

IODA has been built to interface in the operating room with standard equipment and tools used for DBS surgeries pertaining to movement diseases. Figure 2.1 diagrams the overall system integration with the patient and the major components of IODA.

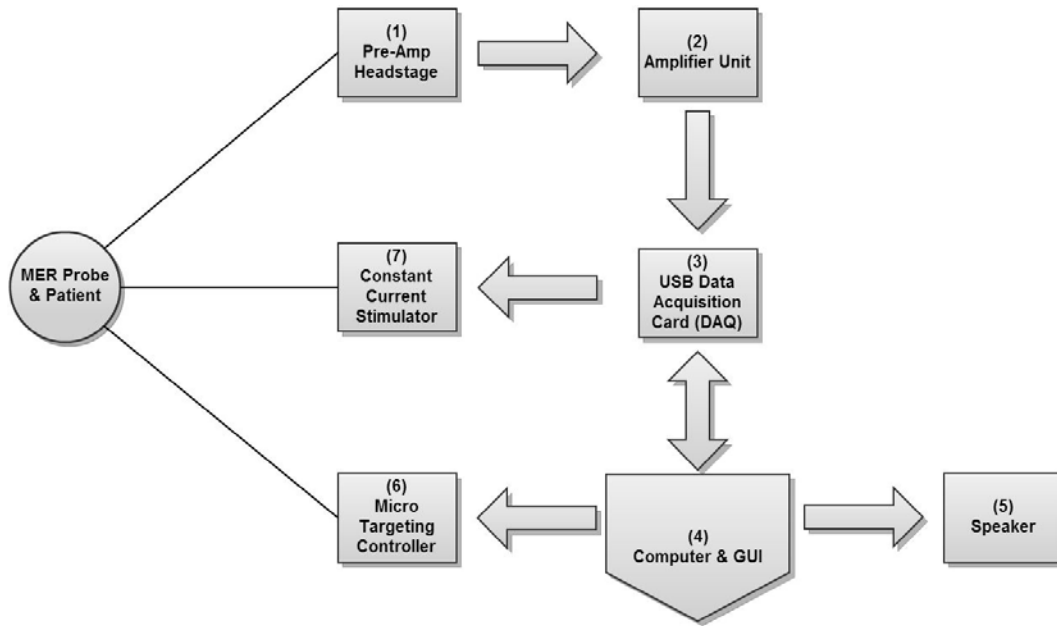


Figure 2.1: IODA Architecture includes amplifier and headstage interface for probes, data acquisition card for analog to digital conversion of signal, probe depth controller, computer for realtime analysis and display, and speaker for audio from neural recording.

The system is comprised of seven major components. The pre-amplifier headstage (1) interfaces with MER probes to capture raw unfiltered differential signals from the patient using a disposable shielded cable (D360 Isolated Patient Amplifier System; Digitimer, London, England). The headstage has 8 available channels each with an impedance of 100 MOhms. The headstage amplifies the neural signal with a gain of 100 prior to passing the signal to the amplifier unit (2) where filtering and further amplification is applied. For our clinical use, the amplifier applied a bandpass filter from 1Hz to 8 kHz and a gain of 10 for a total signal gain of 1000. The amplifier is capable of low-cut, notch, and high-cut filtering using a dynamic range of filter frequency values.

Once filtered, the analog signal is digitally converted using the data acquisition card (DAQ) (3) (Model DT9837A, Data Translation; Marlboro, MA). The DAQ is capable of sampling analog signals from 1Hz – 52 kHz with 24bit resolution with each analog input having an impedance of 1MOhm. For our clinical use, the DAQ sampled the analog signals at 30 kHz to ensure single unit neuronal firing could be recorded without loss. The signal was displayed and digitally filtered further using a commercially available computer (4) (Precision T5500, Dell; Round Rock, TX) and graphical interface (Labview 2010, National Instruments; Austin TX).

Digital filtering was performed for intraoperative audio monitoring (5) of the high frequency band signal (300 Hz – 2 kHz) used for electrophysiological monitoring. The computer is also connected with the microTargeting Controller (MTC) which integrates with the motor that advances the MER probe in the brain (microTargeting Controller, FHC; Bowdoin, ME). The MTC is capable of sub-millimeter movements of the probe and provides the depth of the probe in the brain.

The system is also capable of stimulation through MER probes. The DAQ output is connected to the constant current stimulator (7) (DS4, Digitimer). This stimulator ensures intended amounts of current are applied to neural tissue by varying the required voltage based on measured impedance. This is different from all available stimulating platforms which are constant voltage based stimulators which cannot control for applied energy. The IODA stimulator is able to generate voltages of ± 48 V with output ranges from 1 μ A to 10 mA. Stimulation profiles are sent from the computer to the DAQ which converts the digital signal to analog and passes the signal to the stimulator. The stimulator is isolated and applies current stimulation directly to the MER probe via the shielded cables.

Results

We benchmarked are system capabilities and features with the Guideline 4000 (FHC; Bowdoin, ME) for high frequency recording, micro stimulation (1 μ V -100 μ V), and macro stimulation (1 mV -10 mV). We used previously published methods of signal analysis on recorded LFP signals and compared our results to recent studies in order to ensure wideband recording capabilities of IODA [19, 20]. In addition we demonstrated IODA's ability to create customizable stimulation waveforms for research purposes and a more intuitive GUI.

Wideband Signal Recording

Figure 2.2 shows a brief recording of the HFB signal from the right STN of a Parkinson's disease patient undergoing DBS treatment. An individual spike had amplitude of 115 μ V; which was consistent with physiological STN neuronal spiking amplitudes. The signal was recorded differentially with a 1 MOhm impedance MER probe, analog filtered between 1 Hz and 8 kHz, amplified with a gain = 600, sampled at 30 kHz, then digitally filtered from 300 Hz to 5 kHz.

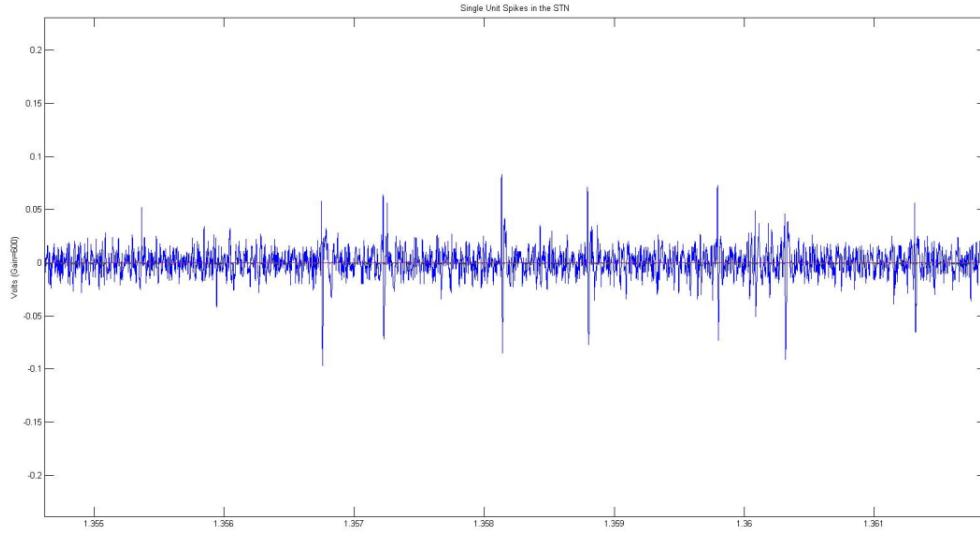


Figure 2.2: A filtered signal recorded from within the STN of a Parkinson disease patient using IODA. This recording was captured using a microelectrode at a fixed depth. The average amplitude of this recorded unit was 115 μ V.

Figure 2.3 illustrates a Gabor power spectrogram of the beta band recorded from LFP signals in the STN of a Parkinson’s disease patient. The signal was recorded differentially with a 1 MOhm impedance MER probe, analog filtered between 1 Hz and 8 kHz, amplified with a gain = 100, sampled at 30 kHz, then downsampled to 500 Hz and digitally filtered from 5 Hz to 30 Hz. The method for LFP analysis and plotting is previously described [19, 20]. There is significant activity in the theta and beta frequency range, consistent with recent studies showing power intensities of the LFP signal in the STN.

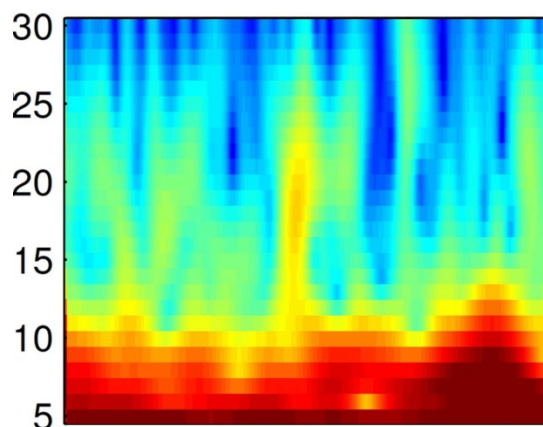


Figure 2.3: A spectrogram of 5 Hz to 30 Hz power in the LFP signal recorded from the STN of a Parkinson disease patient using IODA. Power intensities are normalized for the frequency band. Activation in the beta band (13 Hz to 30 Hz) is seen clearly at 20 Hz.

Noise Floor Amplitude

Figure 2.4 shows the noise floor of IODA. The signal was generated without any neuronal recordings or other signal sources. The average baseline for noise in our surgical setup using IODA was 5 μV .

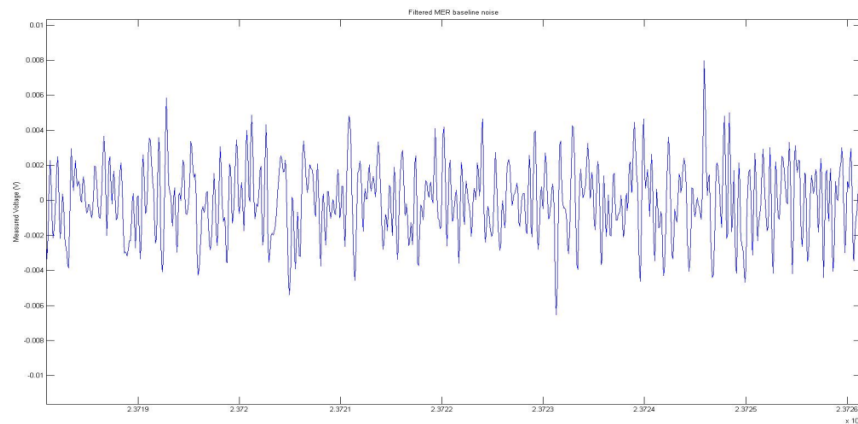


Figure 2.4: The baseline noise for the IODA system turned on and not connected with adjunctive components is 0.5 μV .

Stimulation Capabilities

IODA is capable of providing the standard square wave stimulation waveform with varying pulse widths, frequencies, and amplitudes. Figure 2.5 shows the standard square wave pulse generated from the Medtronic 8840 external stimulation and IODA at amplitude of 2 V, 130 Hz stimulation frequency, and 60 μsecond pulse width.

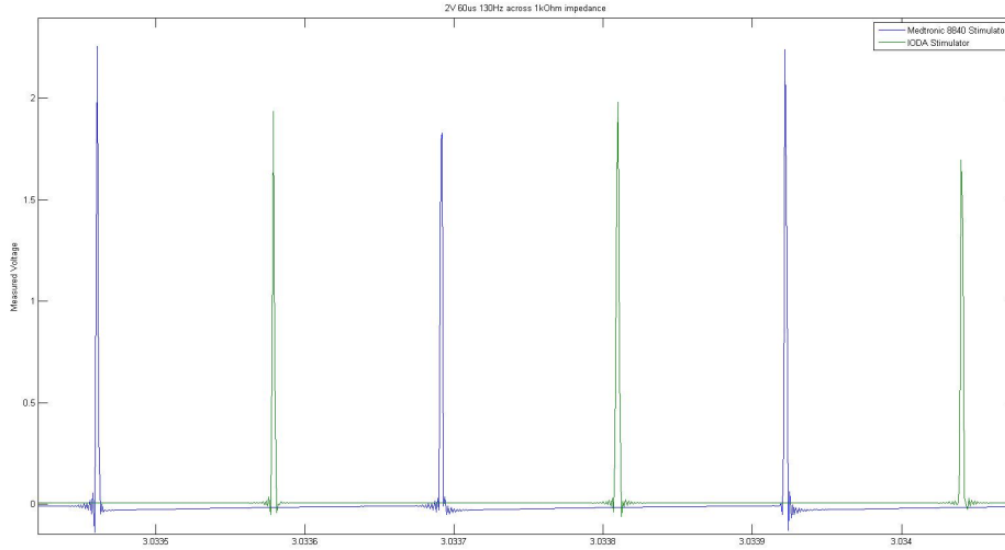


Figure 2.5: Medtronic 8840 (Blue plot) vs IODA stimulator (Green plot) at 2Volts 130 Hz square wave with 60 μ s pulse width. X-axis represents measured voltage and Y-axis represents samples recorded. Medtronic 8840 yielded 2V output, IODA stimulator averaged 2V output.

IODA is also capable of customizable stimulation profiles that vary waveforms, frequencies, pulse widths, and amplitudes. Figure 2.6 shows various stimulation profiles of IODA.

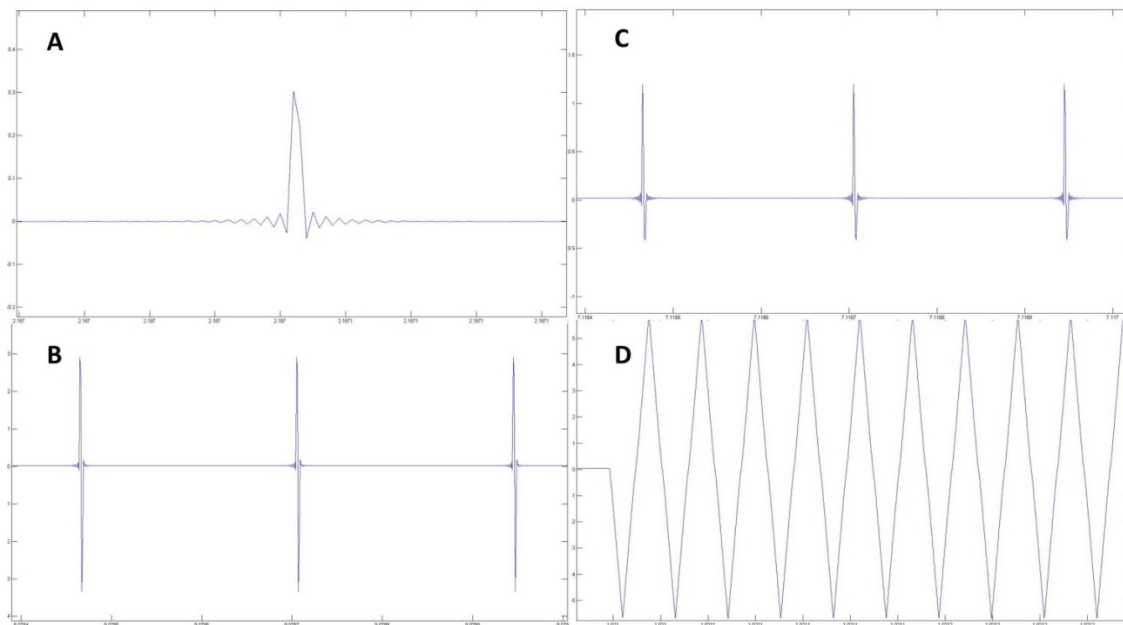


Figure 2.6: Examples of IODA custom stimulation profile capability. A) A single square wave pulse at 130 Hz, 60 μ s pulse width, and a .3 V amplitude shown. B) A custom neuronal spike featured stimulation profile with equal positive (3 V) and negative (-3 V) amplitudes. C) An alternative neuronal spike type stimulation profile with unequal charge output, positive pulse (1 V) and negative pulse (- 0.5 V).

Integration of Research Tools

One of the primary benefits of IODA is the ability to integrate various tools used for DBS research directly into the system. Figure 2.7A shows the direct acquisition of an analog joystick (Freedom 2.4, Logitech; Newark, CA) rotation used during a StopGo movement task. Figure 2.7B shows the recorded signal from a photodiode (Li-210 Photometric Sensor, Li-Cor; Lincoln, NE) placed on the screen during the movement task to track screen changes.

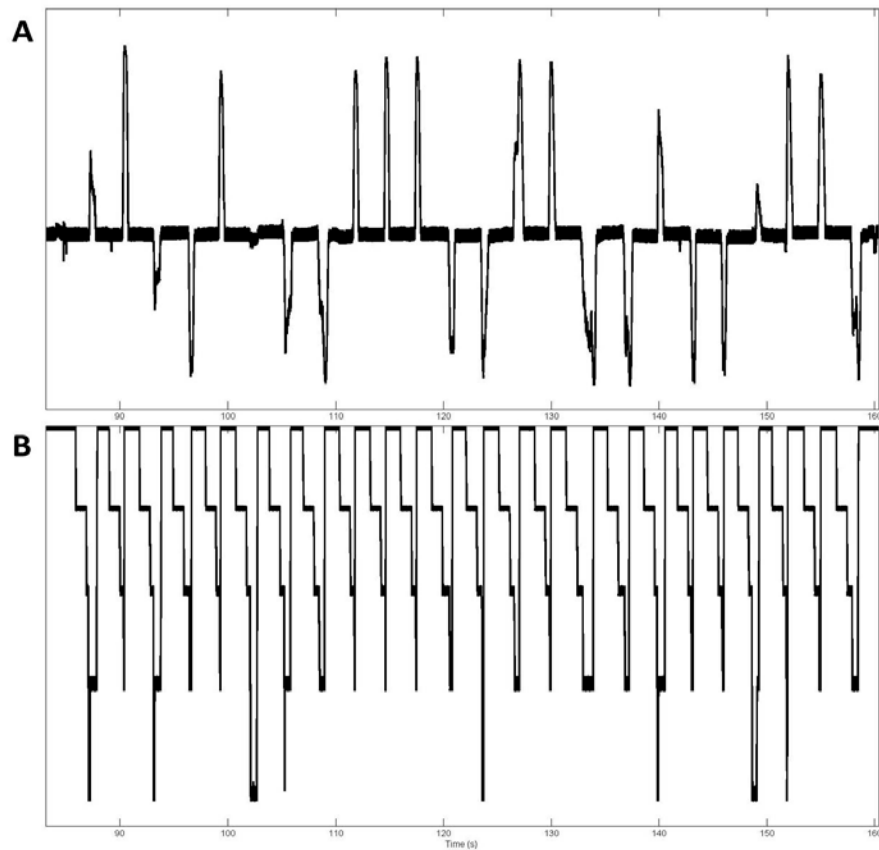


Figure 2.7: Analog data signals from joystick movements and photodiode sensing screen changes during Stop-Signal task recorded intraoperatively during DBS procedure. Both figures show 160 s worth of synced task data. A) Plot for joystick rotations either left (positive) or right (negative) for 24 trials of stop-signal task. B) Photodiode data for 24 trials from stop-signal task with 5 trial events shown. Baseline (top of figure) is start of trial, instruction cue presented to user for either left or right movement (second stage), joystick rotation initiated (end of second stage), stop-signal cue in 8 of 24 trials shown (fourth stage, lowest point), and trial end event is the return of the photodiode signal to baseline.

Graphical User Interface

IODA is designed to provide the user with a traditional electrophysiological view of MER signals as well as a more intuitive primary view using MR images. Figure 2.8 shows the

typical primary view familiar to most intraoperative users. Controls for raw signal views, filters, gains, motor, volume, raw data file writing, experimental tasks, and stimulating are shown. Additionally, IODA provides the user with individual spikes display, a dynamic range for power spectral analysis display, and average power view for multiple frequency bands for each recorded depth.

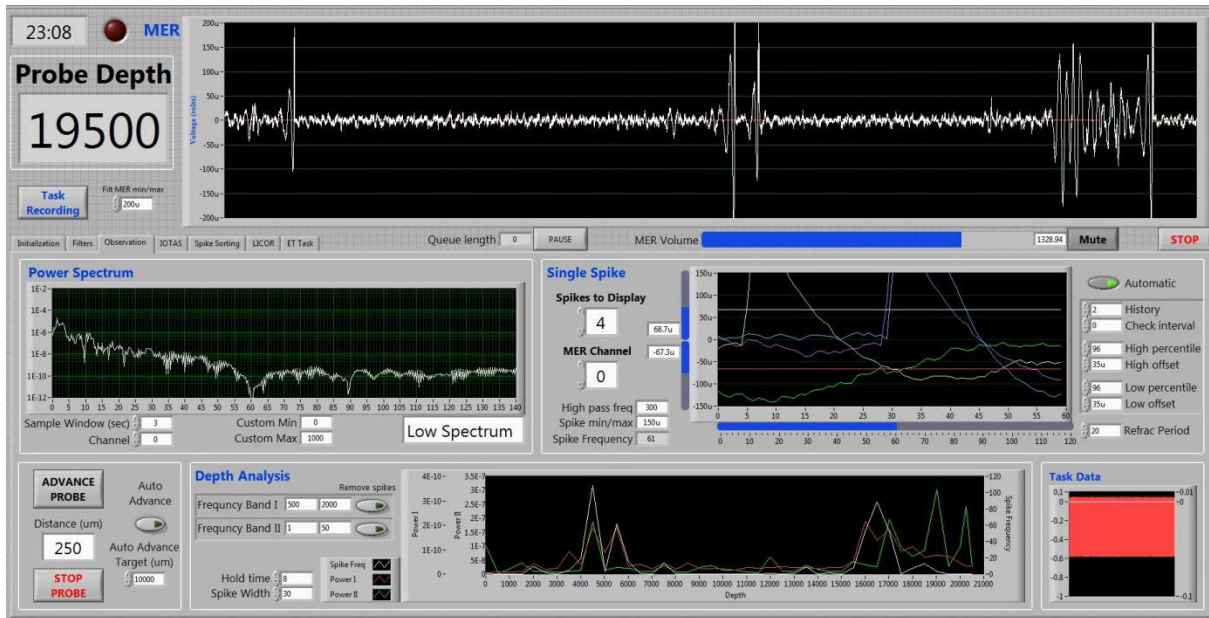


Figure 2.8: Typical electrophysiological display from MER signals. IODA display showing filtered raw signal on top, duration and depth of recording on top left, volume control, adjustable power spectrum, single spike threshold detection, probe motor control, and average power of MER signal at each recording step at bottom of display.

Figure 2.9 is an alternative primary view of intraoperative electrophysiology. Patient MRI files can be loaded and viewed through the GUI. The real-time position of the MER probe can be superimposed on the image to provide an accurate and intuitive visualization of the probe's location in the brain.



Figure 2.9: IODA’s alternate primary electrophysiological view. The display uses the patient’s preoperative MRI image and preoperative CT scan with frame to create an accurate frame-space image. The MER probe is superimposed onto the frame-based MRI image to show a real-time position of the probe as it traverses through the planned trajectory. Audio from the filtered signal is played throughout the trajectory.

Conclusions

We demonstrate a novel system that can be used intraoperatively for data acquisition and neural stimulation during DBS procedures. The present system is capable of providing the information necessary for neurosurgeons and electrophysiologists to perform standard electrophysiological analysis for target localization. In addition, the system is able to be used for research by combining wideband signal recording, various stimulation profiles, medical imaging, and experimental patient tasks. We have developed and verified functionality of IODA in over 75 DBS cases at our institution.

We found our system to provide usable and meaningful data in both the LFP and HFB when used for MER. Our data analysis of both raw single unit activity and LFP activity was compared to recent studies and confirmed our method of acquisition and system setup to be correct. We did find limitations in the signal integrity between the MER probe and pre-amplifier headstage. We observed occasional points of electrical saturation in the amplifier that may have been caused by large potential differences in the anode and cathode contacts of the MER. We

were able to resolve this issue by referencing the anode contact to ground and effectively record in a mono-polar setup. The system amplifier unit was also found to periodically have a ground potential different from that of the MER ground reference. This difference in potential for referenced ground inevitably caused ground loops in our system. We resolved this by isolating each component in our system and referencing only the patient as the sole source for ground references throughout the system.

We also observed similar stimulation effects using the integrated IODA stimulation when compared to the Medtronic 8840 external stimulator and the Guideline 4000. We did find limitations in stimulation capabilities in our system due to variance in electrode impedance. However electrode impedance variability equally affected the other stimulators. In addition, we observed a lower limit threshold for stimulation profiles that required shorter pulse widths than the ranges specified for IODA. This is primarily due to physical hardware constraints in the computer and DAQ clock for μ second pulse widths.

We also demonstrated the capability of intraoperative DBS research using IODA. The system was integrated with a joystick and photodiode sensor to sync a movement related task with neural recordings in the STN. The compatibility of IODA with both sensors enabled a successful research experiment involving Parkinson's patients to further understand the role of the STN in movement related diseases.

IODA was tested intraoperatively with the alternative primary display. Both neurosurgeons and electrophysiologists explicitly expressed the benefits of the intuitive view using MR images and MER audio. Even for experienced users, the primary display for IODA enabled neurosurgeons to reduce surgical time, risk, and targeting error. The real-time update of MER probe position on patient MR images reduces the internal visualization of probe location usually required by neurosurgeons.

We have successfully demonstrated a versatile and powerful intraoperative targeting system for neuromodulation during DBS surgeries. This system can be used for both clinical and research applications during DBS cases. The system can potentially enable neurosurgeons that are not specialty trained to perform DBS and help reduce surgical time and error for experienced users.

References

- [1] A. L. Benabid, S. Chabardes, J. Mitrofanis, and P. Pollak, "Deep brain stimulation of the subthalamic nucleus for the treatment of Parkinson's disease," *Lancet neurology*, vol. 8, pp. 67-81, Jan 2009.
- [2] K. L. Holloway, S. E. Gaede, P. A. Starr, J. M. Rosenow, V. Ramakrishnan, and J. M. Henderson, "Frameless stereotaxy using bone fiducial markers for deep brain stimulation," *Journal of neurosurgery*, vol. 103, pp. 404-13, Sep 2005.
- [3] D. Sterio, M. Zonenshayn, A. Y. Mogilner, A. R. Rezai, K. Kiprovski, P. J. Kelly, and A. Beric, "Neurophysiological refinement of subthalamic nucleus targeting," *Neurosurgery*, vol. 50, pp. 58-67; discussion 67-9, Jan 2002.
- [4] B. P. Bejjani, D. Dormont, B. Pidoux, J. Yelnik, P. Damier, I. Arnulf, A. M. Bonnet, C. Marsault, Y. Agid, J. Philippon, and P. Cornu, "Bilateral subthalamic stimulation for Parkinson's disease by using three-dimensional stereotactic magnetic resonance imaging and electrophysiological guidance," *Journal of neurosurgery*, vol. 92, pp. 615-25, Apr 2000.
- [5] W. D. Hutchison, R. J. Allan, H. Opitz, R. Levy, J. O. Dostrovsky, A. E. Lang, and A. M. Lozano, "Neurophysiological identification of the subthalamic nucleus in surgery for Parkinson's disease," *Annals of neurology*, vol. 44, pp. 622-8, Oct 1998.
- [6] R. E. Gross, P. Krack, M. C. Rodriguez-Oroz, A. R. Rezai, and A. L. Benabid, "Electrophysiological mapping for the implantation of deep brain stimulators for Parkinson's disease and tremor," *Movement disorders : official journal of the Movement Disorder Society*, vol. 21 Suppl 14, pp. S259-83, Jun 2006.
- [7] A. Zaidel, A. Spivak, L. Shpigelman, H. Bergman, and Z. Israel, "Delimiting subterritories of the human subthalamic nucleus by means of microelectrode recordings and a Hidden Markov Model," *Movement disorders : official journal of the Movement Disorder Society*, vol. 24, pp. 1785-93, Sep 15 2009.
- [8] P. Novak, S. Daniluk, S. A. Ellias, and J. M. Nazzaro, "Detection of the subthalamic nucleus in microelectrographic recordings in Parkinson disease using the high-frequency (> 500 hz) neuronal background. Technical note," *Journal of neurosurgery*, vol. 106, pp. 175-9, Jan 2007.
- [9] J. Coste, L. Ouchchane, L. Sarry, P. Derost, F. Durif, J. Gabrillargues, S. Hemm, and J. J. Lemaire, "New electrophysiological mapping combined with MRI in parkinsonian's subthalamic region," *The European journal of neuroscience*, vol. 29, pp. 1627-33, Apr 2009.
- [10] J. J. Lemaire, J. Coste, L. Ouchchane, F. Caire, C. Nuti, P. Derost, V. Cristini, J. Gabrillargues, S. Hemm, F. Durif, and J. Chazal, "Brain mapping in stereotactic surgery: a brief overview from the probabilistic targeting to the patient-based anatomic mapping," *NeuroImage*, vol. 37 Suppl 1, pp. S109-15, 2007.
- [11] P. Brown and D. Williams, "Basal ganglia local field potential activity: character and functional significance in the human," *Clinical neurophysiology : official journal of the International Federation of Clinical Neurophysiology*, vol. 116, pp. 2510-9, Nov 2005.
- [12] N. J. Ray, N. Jenkinson, S. Wang, P. Holland, J. S. Brittain, C. Joint, J. F. Stein, and T. Aziz, "Local field potential beta activity in the subthalamic nucleus of patients with

- Parkinson's disease is associated with improvements in bradykinesia after dopamine and deep brain stimulation," *Experimental neurology*, vol. 213, pp. 108-13, Sep 2008.
- [13] T. Trottenberg, A. Kupsch, G. H. Schneider, P. Brown, and A. A. Kuhn, "Frequency-dependent distribution of local field potential activity within the subthalamic nucleus in Parkinson's disease," *Experimental neurology*, vol. 205, pp. 287-91, May 2007.
- [14] F. Yoshida, I. Martinez-Torres, A. Pogosyan, E. Holl, E. Petersen, C. C. Chen, T. Foltynie, P. Limousin, L. U. Zrinzo, M. I. Hariz, and P. Brown, "Value of subthalamic nucleus local field potentials recordings in predicting stimulation parameters for deep brain stimulation in Parkinson's disease," *Journal of neurology, neurosurgery, and psychiatry*, vol. 81, pp. 885-9, Aug 2010.
- [15] A. A. Kuhn, T. Trottenberg, A. Kivi, A. Kupsch, G. H. Schneider, and P. Brown, "The relationship between local field potential and neuronal discharge in the subthalamic nucleus of patients with Parkinson's disease," *Experimental neurology*, vol. 194, pp. 212-20, Jul 2005.
- [16] C. C. Chen, A. Pogosyan, L. U. Zrinzo, S. Tisch, P. Limousin, K. Ashkan, T. Yousry, M. I. Hariz, and P. Brown, "Intra-operative recordings of local field potentials can help localize the subthalamic nucleus in Parkinson's disease surgery," *Experimental neurology*, vol. 198, pp. 214-21, Mar 2006.
- [17] M. Alavi, J. O. Dostrovsky, M. Hodaie, A. M. Lozano, and W. D. Hutchison, "Spatial extent of beta oscillatory activity in and between the subthalamic nucleus and substantia nigra pars reticulata of Parkinson's disease patients," *Experimental neurology*, Oct 9 2012.
- [18] A. Zaidel, A. Spivak, B. Grieb, H. Bergman, and Z. Israel, "Subthalamic span of beta oscillations predicts deep brain stimulation efficacy for patients with Parkinson's disease," *Brain : a journal of neurology*, vol. 133, pp. 2007-21, Jul 2010.
- [19] Y. Miyagi, T. Okamoto, T. Morioka, S. Tobimatsu, Y. Nakanishi, K. Aihara, K. Hashiguchi, N. Murakami, F. Yoshida, K. Samura, S. Nagata, and T. Sasaki, "Spectral analysis of field potential recordings by deep brain stimulation electrode for localization of subthalamic nucleus in patients with Parkinson's disease," *Stereotactic and functional neurosurgery*, vol. 87, pp. 211-8, 2009.
- [20] D. K. Leventhal, G. J. Gage, R. Schmidt, J. R. Pettibone, A. C. Case, and J. D. Berke, "Basal ganglia beta oscillations accompany cue utilization," *Neuron*, vol. 73, pp. 523-36, Feb 9 2012.

Chapter 3 : An Automated Targeting System for Subthalamic Nucleus Deep Brain Stimulation

Abstract

Background: Accurate localization of the subthalamic nucleus (STN) is critical to the success of deep brain stimulation (DBS) surgery for Parkinson disease. Frame inaccuracies, imaging resolution, and target uncertainties can make STN DBS surgery a challenging procedure, even for specialty trained neurosurgeons.

Objective: To develop a novel method for automatically identifying the location of microelectrode trajectories on magnetic resonance (MR) images based on the relationship between voxel intensities and the high frequency band (HFB) signal from microelectrode recordings (MER).

Methods: We evaluated HFB power changes along 20 MER trajectories in 13 patients. We also found voxel intensity values from 3-T MRI along the preoperatively planned trajectory and the implanted DBS lead trajectory. We compared and scored over 100,000 potential voxel-based trajectories for each MER pass to identify trajectories that best matched the MER data. Top scoring voxel trajectories were averaged to produce best estimates and distances to actual DBS leads were compared to that of planned trajectories.

Results: Targeting certainty was improved in over 70% of evaluated trajectories. The averaged MER trajectory distance ($2.33\text{mm} \pm 0.2\text{mm}$) was significantly closer than the planned trajectory distance ($2.83\text{mm} \pm 0.2\text{mm}$) to the DBS electrode final position ($P = 0.01$). In trajectories that initially missed the STN, subsequent trajectory adjustments were predicted with 100% accuracy in the direction shifted by the attending neurosurgeon.

Conclusion: The location of DBS leads can be better estimated using this method by evaluating the position of a MER trajectory in the STN intra-operatively. This method may also reduce

surgical procedure durations and errors associated with classic neurophysiological analysis by automating the analysis of both imaging and electrophysiology data.

Introduction

Deep brain stimulation (DBS) is a well-established surgical therapy for Parkinson's disease.¹ Bilateral chronic high-frequency stimulation of the subthalamic nucleus (STN) is typically targeted as an ideal location for alleviating the motor symptoms of Parkinson's disease.²⁻⁸ Specifically, the dorsal-lateral region of the STN is traditionally targeted indirectly with standardized stereotactic atlases.^{9, 10} In recent years, direct visualization of the STN with magnetic resonance imaging (MRI) has been possible using a range of magnetic field strengths (1.5T-9.4T). This advancement in imaging has enabled increased visibility of the STN region and has improved the method for preoperatively identifying an optimal target.¹¹

However, significant distortions of the brain do occur during DBS surgery mostly due to the loss of CSF and the buildup of intracranial air.¹² This shifting of the brain anatomy from what is visualized in MR imaging creates a misalignment with the planned target for DBS. For multiple reasons including brain shift, microelectrode recording (MER) is often used intraoperatively to assist in locating the STN.¹³⁻¹⁷ With the advancement of imaging technologies, intraoperative signal analysis from MER has been shown to have good correlation to visualized structural borders, including the STN, from MR images.^{11, 18, 19} In addition, the analysis of high frequency band (HFB) signals from MER can provide quantitative information regarding physiological structures during DBS surgery.^{20, 21}

Even with MER and improved imaging resolution, DBS procedures still lack the ability to precisely locate the microelectrode trajectory intraoperatively in frame-based stereotactic coordinates. Without having exact location coordinates of the microelectrode relative to the planned target, the final placement of the DBS lead could be significantly further from the target location than intended. Typically the average error between the planned target and the actual DBS lead is 3.1 ± 1.41 mm.²² Having a more accurate location of the DBS lead prior to insertion can provide valuable clinical benefit by reducing the error observed between planned and DBS lead trajectories.

It would be useful to provide precise locations of microelectrodes intraoperatively to determine if planned targets have been reached. By providing the final trajectory position of microelectrodes a more accurate location of DBS lead positions is also possible.

We aimed to study electrophysiological signals as they relate to high resolution MR image voxels to provide positional information of microelectrode trajectories relative to the intended target. We hypothesized that by relating the changes in HFB power recorded from microelectrodes to the changes in MRI voxel intensities, a calculated position of the microelectrode can be mapped to a MRI. We measured the distance between the calculated positions of the microelectrode to the DBS lead compared to the distance between the planned trajectory targets to the DBS lead in order to determine if the calculated MER trajectory was more closely aligned to the DBS lead than the planned trajectory (Figure 3.1). Since the DBS lead travels in the same trajectory as the final trajectory of the MER, we expected the calculated position of the microelectrode to be significantly closer to the DBS lead than the planned trajectory.

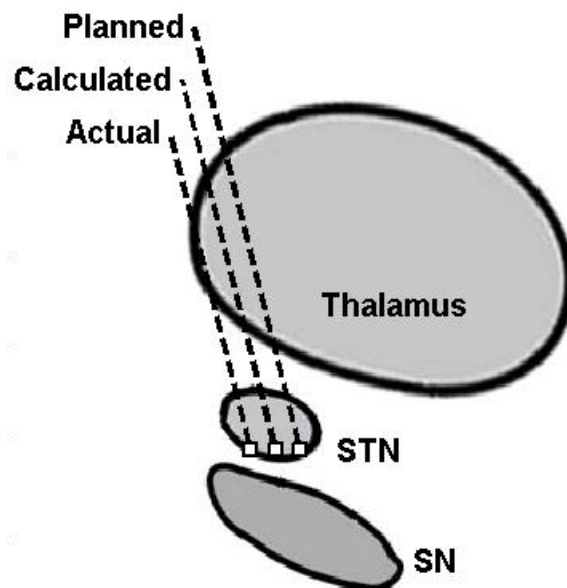


Figure 3.1: Experimental method showing actual DBS lead trajectory, calculated MER trajectory, and planned trajectory targeted for STN with thalamus and substantia nigra (SN) also shown.

Methods

Patient Selection

We studied 13 consecutive patients with advanced idiopathic Parkinson disease who underwent STN DBS surgery at our institution (9 men, 4 women; age, 66 ± 6 years; range, 52-73 years). Patient selection criteria for DBS has been previously described.¹¹ Briefly, selected patients were diagnosed with Parkinson disease and had motor fluctuations not controlled well by

medications or had levodopa-unresponsive tremor. Patients were excluded from this study if contraindications to 3-T MRI scanning or abnormalities in brain anatomy existed. We performed the study in accordance with the policies of the Medical Institutional Review Board of the University of Michigan.

DBS Procedure

The DBS procedure used in this study has previously been described.¹¹ Briefly, all patients underwent 3-T MRI using a coronal imaging protocol designed for visualization of the STN. Patients were fitted with a Leksell stereotactic frame (Elekta Instruments AB, Stockholm, Sweden) and underwent a preoperative 1.5-T MRI the day of surgery. Both 3-T and 1.5T MR images were coregistered using a mutual-information algorithm (Analyze 9.0; AnalyzeDirect, Inc, Overland Park, Kansas). Frame-based bilateral surgical targeting was then performed with commercial software (Framelink; Medtronic, Inc, Minneapolis, Minnesota). Initial indirect targeting at 12 lateral, 3 posterior, and 4 inferior to the midcommissural point was performed and then fine-tuned to the individual patient according to the MR-visualized STN.

During surgery, MER was performed prior to the insertion of the DBS lead for target localization. Neural signals were recorded using a bipolar microelectrode (MicroTargeting Electrode; FHC, Bowdin, ME) advanced during surgery using a microdrive (MicroTargeting Controller; FHC, Bowdin, ME). The initial position of the microelectrode was set to 15mm above the planned target. The microelectrode was advanced in 0.5mm steps and held for 8 seconds to record extracellular signals. MER signals were amplified with a gain between 100-1000 (D360 Isolated Patient Amplifier System; Digitimer Inc, Hertfordshire, England) and recorded to a computer with custom software (LabView 10.1; National Instruments, Austin, TX) using a USB data acquisition card (Model DT9837A; Data Translations Inc, Marlboro, MA). The hold time for MER recordings at each step was selected to maximize recorded HFB signals while minimizing overall surgical procedure duration. Step sizes were shortened to 0.1-0.4mm when in the proximity of the STN. The STN dorsal and ventral borders were identified by an electrophysiologist. DBS leads were placed under fluoroscopic visualization with the tip of the DBS lead located near the ventral border of the electrophysiological STN. A movement disorders neurologist activated the DBS electrodes intraoperatively and evaluated the patient for symptom improvements and side effects. After several weeks, allowing intracranial air to

resolve, a high-resolution postoperative computed tomography (CT) scan was performed to visualize the location of the DBS leads within the brain.

MER Signal Processing

Microelectrode recordings were filtered using a 500Hz to 2000Hz bandpass filter and sampled at a rate of 30kHz (LabView 10.1; National Instruments, Austin, TX). Recordings for each trajectory were saved as double precision values in a computer for offline analysis.

In order to calculate average power of the HFB based on neuronal background activity, large spikes recorded near the microelectrode were removed with a cutoff threshold of ± 50 microVolts. The threshold was set based on our recorded spikes having amplitudes greater than ± 80 microVolts. Trajectories that had significant or sustained areas of noise were omitted from this analysis.

The power spectral density was calculated over the 8-second recorded segments for each depth with a Fourier transform of 15000 samples per segment weighted by a hamming window. The average power in the frequency domain for the HFB was analyzed for each recorded depth using software written in Matlab (Version 2012b; The Math Works, Inc., Natick, MA). Each HFB average power value was normalized at every recorded depth to generate a normalized MER trajectory of average power.

Image Analysis

Details of our 3-T MR and CT imaging protocols have been previously described.¹¹ Trajectory coordinates for implanted DBS lead position were identified from postoperative CT scans co-registered to the 3-T MRI using a mutual-information algorithm (Analyze 9.0). We used DBS leads with 1.5 mm contact lengths and 0.5 mm spacing between contacts (Model 3889, Medtronic; Minneapolis, MN). All voxel intensities were selected from 3-T MR images with a voxel resolution of (0.5mm \times 0.5mm \times 0.5mm). Voxel intensity values were inverted to represent physiological structures and normalized for each trajectory. Low intensity values on our MR protocol represent darker, denser structures; however electrophysiological analysis has higher power values in more dense structures.^{19,21} Therefore, for each voxel intensity trajectory, voxel intensities were inverted to match the electrophysiological representation of the trajectory.

Selection of Potential Voxel-Based Trajectories

Potential voxel trajectories were selected by creating a search window between two cubes ($8 \text{ voxels} \times 8 \text{ voxels} \times 8 \text{ voxels}$), with one cube centered on the entry coordinate and the other cube centered on the target coordinate of the planned trajectory. Potential trajectories were created by varying entry coordinates in the search cube, varying target coordinates in search cube, or both. Potential trajectory selection criteria included only trajectories of the same length as that of the MER trajectory and trajectories that were within a ± 3 degree range for both the ring and arc angles of the planned trajectory. For an average MER trajectory of length 20mm this method resulted in over 100,000 potential trajectories within 8 voxels of the planned trajectory. Each potential trajectory had entry and exit coordinate recorded as well as the inversed normalized voxel intensities along its trajectory at every recorded depth. Figure 3.2A shows an example of this selection method using three potential voxel-based trajectories and the respective inverse voxel intensity plots. Figure 3.2B visualizes the search window and potential voxel trajectories on the coronal view of a targeted STN.

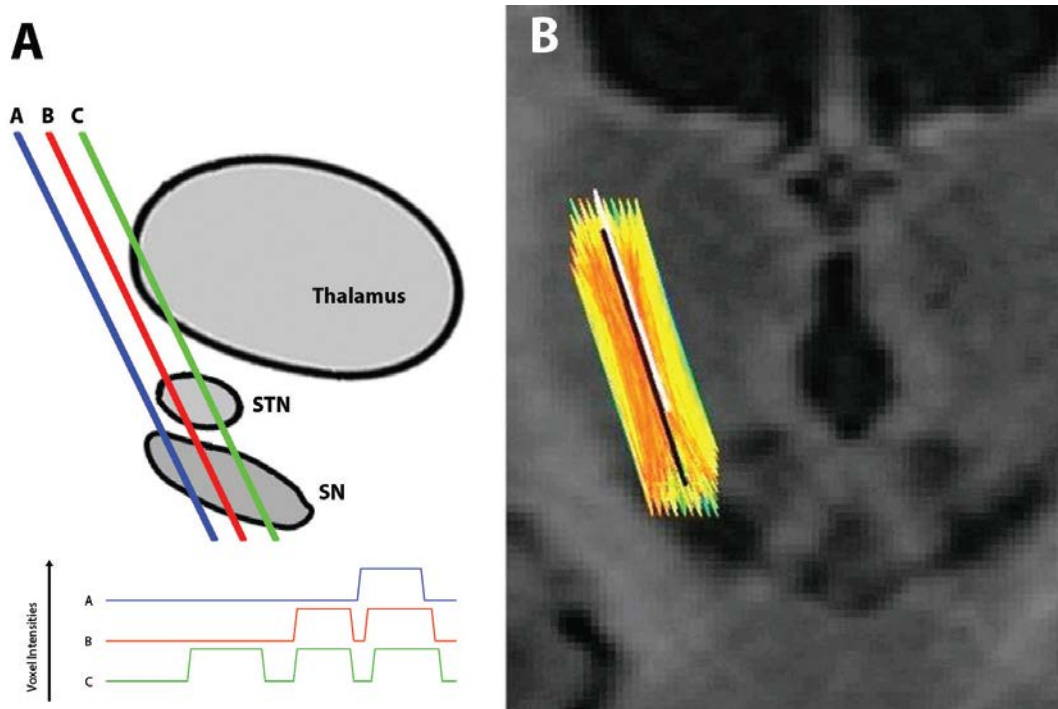


Figure 3.2: A) Potential trajectories and the associated intensities along each track through thalamus, subthalamic nucleus, and substantia nigra (SN) shown. B) 3-T MRI coronal view of STN targeted potential voxel trajectories in an 8 voxel search window. 110,000 trajectories shown with score indicated by color (Red = high score, Green = low score). The black line is the average Top 7% of active trajectories and the white line is the preoperatively planned trajectory.

Scoring Each Potential Voxel Intensity Trajectory to HFB Power Trajectory

The scoring method used voxel based MER trajectory estimates to compare voxel intensities to the observed HFB power data from the MER trajectory. The best voxel trajectory estimate was based on the average of the top scoring voxel trajectories in rank order. Scores were determined by using the sum of absolute errors at every recorded step between each voxel trajectory and the recorded HFB MER trajectory.

A score from 0 to 1 was assigned for each normalized voxel trajectory compared to the normalized HFB power trajectory. Potential voxel trajectories that were well aligned with the HFB power trajectory had small deviations at every recorded depth and therefore had high scores. Potential voxel trajectories with large deviations from the HFB power trajectory had relatively lower scores. Figure 3.3 shows the distribution of scores for potential voxel trajectories of an individual MER trajectory analysis. After all potential trajectories were scored, the results were sorted based on score and the top 7% of trajectories were averaged for a representative average trajectory estimate. A regression analysis was used across all sorted trajectory data to identify the percentile that best minimized the distance between the average trajectory and the final electrode position.

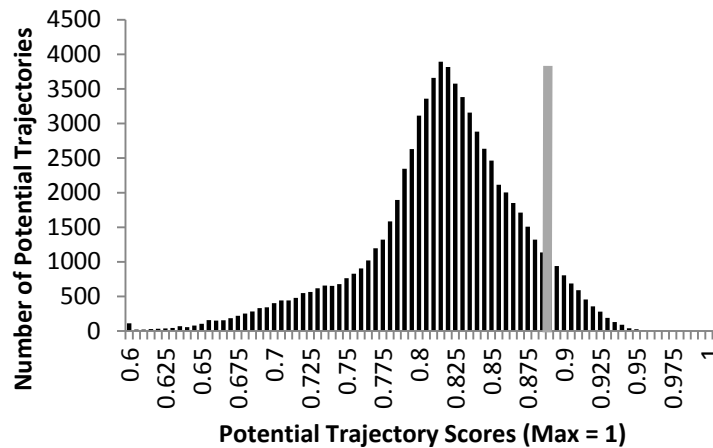


Figure 3.3: Distribution of potential voxel trajectory scores for an individual MER track. The top 7% of trajectories (scores ≥ 0.886) marked with grey vertical line.

Validation of Scoring Method

To validate our scoring method we tested for accuracy in both scoring and location of the analyzed potential voxel trajectories. We first selected a test trajectory and found the voxel intensities along the vector that defined that trajectory. We scored potential voxel trajectories

compared to the test using the test trajectory’s voxel intensities instead of HFB power data from MER. This ensured that the voxels of the test trajectory were within our search window. As expected, the scoring method successfully identified the test trajectory among the potential voxel trajectories in the search window as the top scoring trajectory (score = 1) with 0 mm calculated deviation from the test trajectory. We had the same results when repeated in all MR images used for this study. Figure 3.4 shows the results of this first simulation, labeled ‘No Shift’.

We additionally tested for accuracy in location by intentionally shifting the test trajectory and comparing the resulting potential trajectory scores and locations to this shifted test trajectory. We first intentionally shifted the test trajectory by 1.02 mm (2 voxels) and found the associated voxel intensities that defined this vector. We scored potential trajectories in the same search window as the first test but used the shifted-test voxel intensities instead of the test intensities. The scoring method correctly found the shifted trajectory within the potential voxel trajectories at a deviation from the original test trajectory of 1.02 mm. The results were consistent across all the MR images in our study. We repeated this test using a shift of 1.4mm and found the method to correctly locate the shifted trajectory 1.4mm away from the original test. Figure 3.4 displays these tests between intended shift and calculated shift.

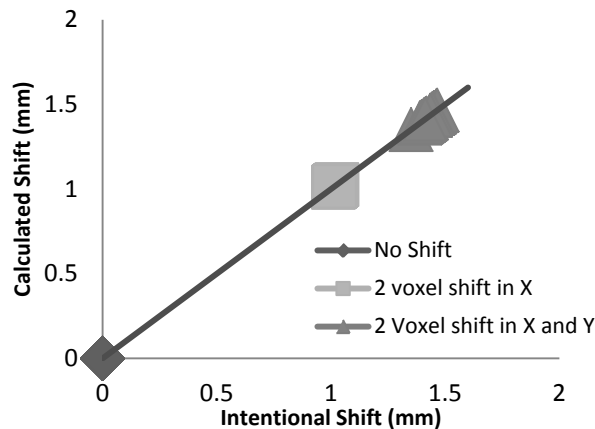


Figure 3.4: Scoring Method Simulation: Intentional shifts of 0mm, 1.02mm, 1.4mm from original test trajectory against the calculated shifts from the scoring method. In all cases (N = 13 patient MR images), the calculated shifts were equal to the intended shifts for each shift test.

Statistical Analysis

Statistical analysis was performed with commercially available software (Matlab 2012b; The Math Works, Inc., Natick, MA, Excel; Microsoft Inc, Redmond, WA). Paired two tailed t-tests were used to calculate p-values for trajectory data comparing averaged trajectory distances

to planned trajectory distances. Distances between the DBS electrode trajectory, planned trajectory, and averaged calculated trajectory were calculated at the Z coordinate of the planned target. Distances in millimeters represent the two dimensional distance of the X and Y coordinates at the planned Z coordinate for every trajectory. Results are reported as mean \pm SEM unless otherwise noted.

Results

A total of 20 STN targeted trajectories from 13 PD patients were available for analysis. Of these, 14 trajectories were final trajectories representing the final trajectory of the DBS electrode. Four of the available trajectories represented a first pass MER trajectory with the subsequent pass moved from the initial position and considered the final trajectory. Two trajectories from two patients were omitted due to DBS lead position change after intra-operative testing yielded poor symptom control.

The average deviations from the DBS lead for the planned and automatically calculated trajectories on a typical STN targeted trajectory were compared for significance. The distance between the averaged top 7% calculated trajectories and the DBS lead was $2.33 \pm 0.2\text{mm}$. The distance between the plan trajectory and the DBS lead was $2.83 \pm 0.2\text{mm}$. A paired t-test revealed that the calculated trajectories were significantly closer to the DBS lead than the planned trajectories for each patient trajectory ($P = .01$).

Figure 3.5 shows a significant correlation between the calculated deviations of the estimated MER trajectory and the measured deviation of the planned trajectory to the DBS lead ($R = .58$, $P = .02$). Of the final 14 trajectories, 10 showed a significant reduction in distance from the actual DBS lead position and 2 trajectories had no significant difference compared to the planned trajectory distance to the DBS lead.

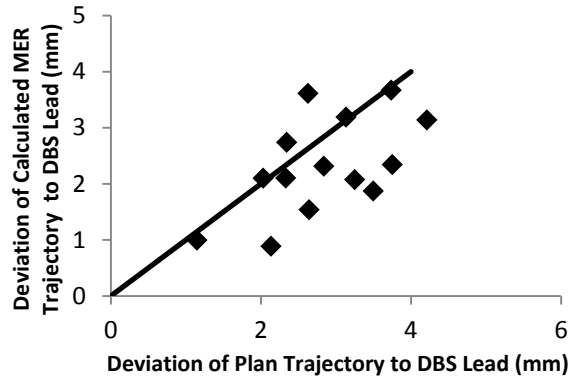


Figure 3.5: Correlation of Planned trajectory and Estimated MER trajectory distances from actual DBS lead. A majority of calculated trajectories were closer to the actual lead position than were planned.

Figure 3.6 shows the distances in the X and Y direction of the top 7% average and plan trajectories to the DBS lead. The Y-coordinate of the top 7% trajectories ($Y = .80 \pm .50$ mm) was significantly closer to the DBS lead than the plan trajectory ($Y = 1.52 \pm .50$ mm, $P < .001$). There was a trend in the X-coordinate of the top 7% trajectories ($X = .43 \pm .35$ mm) to be closer to the DBS lead than the plan trajectory ($X = .62 \pm .42$ mm, $P = .19$).

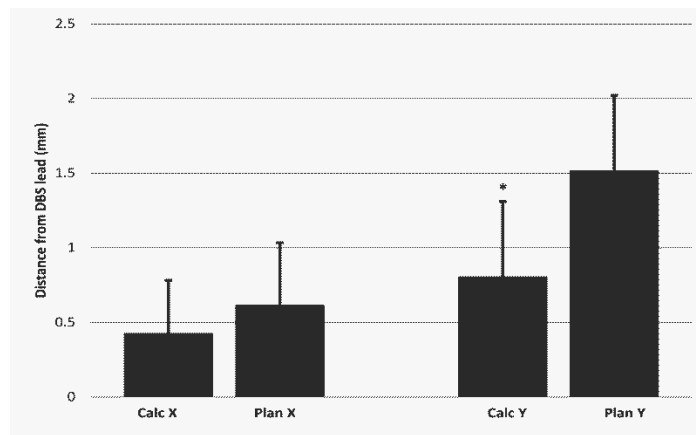


Figure 3.6: Distances from DBS lead in X and Y direction for calculated and plan trajectories compared to show significant reduction in calculated trajectory distance. The Y-coordinate of the calculated trajectory was significantly smaller than the Y-coordinate of the plan trajectory.

We also evaluated the four first pass MER tracks with our scoring method to determine if the direction and magnitude of adjustment of the subsequent final trajectory could be predicted. The average adjustment made by the neurosurgeon after each of these tracks was 2 ± 0 mm anterior of the first pass. The automated scoring method calculated the correct directional shift

but with a smaller magnitude than that of the neurosurgeon, 0.46 ± 0.1 mm in the anterior direction.

Discussion

The effectiveness of STN DBS surgery for Parkinson's disease is dependent on the accuracy of targeting the STN. Targeting the STN traditionally involves using an imaging method to define an initial target estimate and then using intraoperative MER and clinical testing to optimally reposition the electrode. The advancement of imaging technologies has enabled direct visualization of the STN and has accounted for improved targeting methods.^{11, 19} However, during surgery the brain shifts and preoperatively planned targets are also shifted. To account for this, subjective and quantitative analysis of HFB signals from MER enable trained neurosurgeons to determine the location of the microelectrode.^{20, 21, 23}

In this study, we used 3-T MRI voxel intensities and quantitative analysis of the HFB signal obtained during DBS surgery to better estimate the location of the microelectrode trajectory for patients with Parkinson Disease. These results demonstrated that the calculated MER trajectory was significantly closer to the DBS lead than the planned trajectory was to the DBS lead. In this study, one limitation to our measure of accuracy was the surgical uncertainties of final lead placement. The distance between the calculated and actual trajectories was primarily caused by deviations of the DBS lead after insertion through the guiding cannula. Although the cannula provides a rigid path for the DBS lead to travel, there are typically slight deviations between the end of the cannula and target depth.

A basic scoring method was used to evaluate potential voxel trajectories compared to the HFB power signal recorded from MER. This method was validated to ensure accurate scores and locations were assigned to each potential voxel trajectory. We found this method to be robust and efficient when tested with known trajectory locations. In every test of fixed and variable trajectory locations, the scoring method correctly identified the known trajectory out of the over 100,000 potential trajectories analyzed. For our study, we chose a large enough search window to account for the observed error between the planned target and the DBS lead (2.83 ± 0.2 mm). We confined our search space for potential trajectories to approximately 4 mm. This may have limited our study from verifying our results with larger search windows.

Interestingly, of the available MER trajectories for analysis in our study, four were categorized as first tracks. These were trajectories that did not provide sufficient

electrophysiological confirmation of the STN and thus required a subsequent MER track in an alternative location. The automated method provided the information necessary to determine the direction to shift the subsequent MER trajectory, i.e. a shift anterior, posterior, medial, or lateral of the planned target. However, due to the limited resolution (2 mm shifts) and direction of adjustment in our surgical setup we were unable to draw any significant results regarding the magnitude of shift necessary to reach the intended target.

This method could potentially be used to automate and visualize the MER process while possibly reducing surgical time, risk, and error. It may also enable neurosurgeons that are not specially trained to perform DBS procedures by automating the analysis of MER and targeting. Although our study data suggests that calculating the position of a microelectrode with HFB and image analysis may be performed automatically without the need to analyze either, this method cannot completely replace intraoperative electrophysiological monitoring given that intraoperative clinical testing is necessary to confirm that the electrode location is clinically effective.

Conclusion

With the advancements in MRI technology and the quantitative analysis of HFB electrophysiology signals, we show a new method for locating and visualizing a microelectrode intraoperatively. We used 3-T MRI voxel intensities and quantitative analysis of the HFB signal from MER to better estimate the locations of microelectrode trajectories for patients with Parkinson's disease. These results demonstrated that the calculated position of the MER trajectory was significantly closer to the DBS lead than the planned trajectory was to the DBS lead. These results indicate that this method may provide significant improvement to DBS lead placement, surgical error, and surgical duration compared to current methods of DBS targeting.

References

1. Benabid AL, Chabardes S, Mitrofanis J, Pollak P. Deep brain stimulation of the subthalamic nucleus for the treatment of Parkinson's disease. *Lancet Neurol*. Jan 2009;8(1):67-81.
2. Krack P, Benazzouz A, Pollak P, et al. Treatment of tremor in Parkinson's disease by subthalamic nucleus stimulation. *Mov Disord*. Nov 1998;13(6):907-914.
3. Benabid AL, Pollak P, Gross C, et al. Acute and long-term effects of subthalamic nucleus stimulation in Parkinson's disease. *Stereotact Funct Neurosurg*. 1994;62(1-4):76-84.
4. Krack P, Pollak P, Limousin P, Benazzouz A, Benabid AL. Stimulation of subthalamic nucleus alleviates tremor in Parkinson's disease. *The Lancet*. 1997;350(9092):1675.
5. Kumar R, Lozano AM, Kim YJ, et al. Double-blind evaluation of subthalamic nucleus deep brain stimulation in advanced Parkinson's disease. *Neurology*. 1998;51(3):850-855.
6. Lang AE. Surgery for Parkinson disease: A critical evaluation of the state of the art. *Arch Neurol*. Aug 2000;57(8):1118-1125.
7. Rodriguez-Oroz MC, Zamarbide I, Guridi J, Palmero MR, Obeso JA. Efficacy of deep brain stimulation of the subthalamic nucleus in Parkinson's disease 4 years after surgery: double blind and open label evaluation. *J Neurol Neurosurg Psychiatry*. Oct 2004;75(10):1382-1385.
8. Liang GS, Chou KL, Baltuch GH, et al. Long-term outcomes of bilateral subthalamic nucleus stimulation in patients with advanced Parkinson's disease. *Stereotact Funct Neurosurg*. 2006;84(5-6):221-227.
9. Trottenberg T, Kupsch A, Schneider GH, Brown P, Kuhn AA. Frequency-dependent distribution of local field potential activity within the subthalamic nucleus in Parkinson's disease. *Exp Neurol*. May 2007;205(1):287-291.
10. Schaltenbrand G, Wahren W, Hassler R. *Atlas for stereotaxy of the human brain*. 2nd rev. and enl. ed. Stuttgart: Thieme, / Chicago : Year Book Medical Publishers; 1977.
11. Patil PG, Conrad EC, Aldridge JW, Chenevert TL, Chou KL. The anatomical and electrophysiological subthalamic nucleus visualized by 3-T magnetic resonance imaging. *Neurosurgery*. Dec 2012;71(6):1089-1095; discussion 1095.
12. Hunsche S, Sauner D, Maarouf M, et al. Intraoperative X-ray detection and MRI-based quantification of brain shift effects subsequent to implantation of the first electrode in bilateral implantation of deep brain stimulation electrodes. *Stereotact Funct Neurosurg*. 2009;87(5):322-329.
13. Holloway KL, Gaede SE, Starr PA, Rosenow JM, Ramakrishnan V, Henderson JM. Frameless stereotaxy using bone fiducial markers for deep brain stimulation. *J Neurosurg*. Sep 2005;103(3):404-413.
14. Starr PA, Christine CW, Theodosopoulos PV, et al. Implantation of deep brain stimulators into the subthalamic nucleus: technical approach and magnetic resonance imaging-verified lead locations. *J Neurosurg*. Aug 2002;97(2):370-387.
15. Bejjani BP, Dormont D, Pidoux B, et al. Bilateral subthalamic stimulation for Parkinson's disease by using three-dimensional stereotactic magnetic resonance imaging and electrophysiological guidance. *J Neurosurg*. Apr 2000;92(4):615-625.
16. Sterio D, Zonenshayn M, Mogilner AY, et al. Neurophysiological refinement of subthalamic nucleus targeting. *Neurosurgery*. Jan 2002;50(1):58-67; discussion 67-59.

17. Hutchison WD, Allan RJ, Opitz H, et al. Neurophysiological identification of the subthalamic nucleus in surgery for Parkinson's disease. *Ann Neurol*. Oct 1998;44(4):622-628.
18. Hamani C, Richter EO, Andrade-Souza Y, Hutchison W, Saint-Cyr JA, Lozano AM. Correspondence of microelectrode mapping with magnetic resonance imaging for subthalamic nucleus procedures. *Surg Neurol*. Mar 2005;63(3):249-253; discussion 253.
19. Coste J, Ouchchane L, Sarry L, et al. New electrophysiological mapping combined with MRI in parkinsonian's subthalamic region. *Eur J Neurosci*. Apr 2009;29(8):1627-1633.
20. Novak P, Daniluk S, Elias SA, Nazzaro JM. Detection of the subthalamic nucleus in microelectrographic recordings in Parkinson disease using the high-frequency (> 500 hz) neuronal background. Technical note. *J Neurosurg*. Jan 2007;106(1):175-179.
21. Novak P, Przybyszewski AW, Barborica A, Ravin P, Margolin L, Pilitsis JG. Localization of the subthalamic nucleus in Parkinson disease using multiunit activity. *J Neurol Sci*. Nov 15 2011;310(1-2):44-49.
22. Starr PA, Martin AJ, Ostrem JL, Talke P, Levesque N, Larson PS. Subthalamic nucleus deep brain stimulator placement using high-field interventional magnetic resonance imaging and a skull-mounted aiming device: technique and application accuracy. *J Neurosurg*. Mar 2010;112(3):479-490.
23. Gross RE, Krack P, Rodriguez-Oroz MC, Rezai AR, Benabid AL. Electrophysiological mapping for the implantation of deep brain stimulators for Parkinson's disease and tremor. *Mov Disord*. Jun 2006;21 Suppl 14:S259-283.

Chapter 4 : Subthalamic Beta Activity and Optimal Deep Brain Stimulation Sites Spatially Dependent

Abstract

Objective: Deep brain stimulation (DBS) of the subthalamic nucleus (STN) is an effective therapy for Parkinson's disease (PD). However, optimal stimulation sites of the STN region are frequently contested. The aim of this study was to corroborate results from conflicting studies by providing evidence that the relationship between sites of beta hypersynchrony and optimal stimulation are spatially dependent relative to the STN region.

Method: We measured local field potential (LFP) activity in the beta band from 26 subthalamic regions in 13 patients undergoing DBS treatment for PD. We recorded beta LFP data from microelectrodes between 2 mm above the electrophysiological STN to the ventral border and assessed the peak power in the beta band from each recording. 3-T magnetic resonance imaging (MRI) was used to identify the midpoint of the STN. We used postoperative MRI to locate each trajectory relative to the midpoint and the location of the independently chosen contact for chronic stimulation.

Results: Trajectories categorized as medial to the STN midpoint had locations of peak beta power correlated with optimal sites of stimulation. Conversely, trajectories categorized as lateral had locations of peak beta power significantly below optimal contact sites. The optimal contact sites correlated with the dorsal border of the STN in both medial and lateral trajectories.

Interpretation: These results suggest that there is a dependence on location within the STN when using areas of peak beta activity to determine sites of optimal stimulation for DBS in PD patients. These results may have further implications in studies modeling STN beta oscillations, post-operative stimulation parameter selections, and closed-loop stimulation technologies.

Introduction

Deep brain stimulation (DBS) is a well-established surgical therapy for Parkinson's disease.¹ Bilateral chronic high-frequency stimulation of the subthalamic nucleus (STN) alleviates the motor symptoms of Parkinson's disease.²⁻⁸ However, within the STN region there is little consensus as to the most optimal site for chronic stimulation by the active contact of the implanted DBS lead.

Recent studies have presented evidence suggesting excessive synchronization of the beta frequency band (13-30Hz) in the basal ganglia in patients with Parkinson's disease.⁹⁻¹² Additionally, it has been shown that the peak power of the beta signal occurs in the sensorimotor region of the STN, generally observed as the dorsal region of the STN.^{9, 13-17} Increasing evidence points to locations of peak beta activity as the most optimal sites for stimulation in the STN region.¹⁸⁻²² Conversely, it was reported that sites of peak beta power are more centrally located within the STN and therefore may be a poor indicator for optimal stimulation sites.²³ Independent of locations of peak beta hypersynchrony, others have reported the dorsal border of the STN (DB-STN) to be the most optimal location for chronic stimulation based on postoperative clinical effect.^{24, 25} However, there are significant methodological differences in many of these studies ranging from variations in local field potential (LFP) recordings, poor spatial resolution during signal recording, and low imaging resolution for confirmation of trajectory location.

Typically, microelectrode recordings (MER) are used intraoperatively to assist in locating the electrophysiological STN.²⁶⁻³⁰ Signals recorded through microelectrodes range in frequency and enable neurosurgeons to use electrophysiological methods to identify signature neuronal and local field potential (LFP) activity near the STN.³¹ In this study, the STN borders were electrophysiologically identified using MER. Beta LFP signals were recorded using the microelectrode from 2mm above the DB-STN to the ventral border of the STN in 0.1 to 0.4 mm increments. By recording LFPs with microelectrodes, spatial resolution is significantly improved compared to the relatively large electrode contact sites of DBS leads used in previous studies.^{17, 21}

In recent years, improved targeting has been possible through direct visualization of the STN with advancements in magnetic resonance (MR) imaging (MRI).³²⁻³⁴ Direct visualization of the STN has also enabled increased spatial resolution for analysis between trajectory locations and target sites within the STN.^{9, 13-17} Previous studies relating beta power to optimal stimulation sites have lacked the resolution necessary to precisely locate beta trajectories relative to the STN. Although beta power has been shown to vary dorso-ventrally in the STN, it is still unclear whether there is a significant difference in beta power profiles medio-laterally and antero-posteriorly in the STN region.

We hypothesize that the discrepancies seen in recent findings between peak beta power sites and optimal stimulation locations can be explained by differences in LFP recorded trajectory locations relative to the STN midpoint using high resolution MR imaging. In this study, we first demonstrated our LFP recording method by showing similar beta power trends as those observed in comparable studies. We then categorized each LFP trajectory based on its relative location to the midpoint of the visualized STN to show how contested claims regarding beta and optimal stimulation sites are corroborated depending on the trajectory location in the STN region.

Methods

Patient Selection

We studied 13 consecutive patients with advanced idiopathic Parkinson disease who underwent STN DBS surgery at our institution (9 men, 4 women; age, 66 ± 6 years; range, 52-73 years). Patient selection criteria for DBS has been previously described in Patil et al.³³ Briefly, selected patients were diagnosed with Parkinson disease and had motor fluctuations not well controlled by medications or had levodopa-unresponsive tremor. Patients were excluded from this study if contraindications to 3-T MRI scanning or abnormalities in brain anatomy existed. We performed the study in accordance with the policies of the Medical Institutional Review Board of the University of Michigan.

DBS Procedure

The DBS procedure used in this study has previously been described.³³ Briefly, all patients underwent 3-T MRI using a coronal imaging protocol designed for visualization of the

STN. Patients were fitted with a Leksell stereotactic frame (Elekta Instruments AB, Stockholm, Sweden) and underwent a preoperative 1.5-T MRI the day of surgery. Both 3-T and 1.5T MR images were coregistered using a mutual-information algorithm (Analyze 9.0; AnalyzeDirect, Inc, Overland Park, Kansas). Frame-based bilateral surgical targeting was then performed with commercial software (Framelink; Medtronic, Inc, Minneapolis, Minnesota). Initial indirect targeting at 12 lateral, 3 posterior, and 4 inferior to the midcommissural point was performed and then fine-tuned to the individual patient according to the MRI-visualized STN.

During surgery, MER was performed prior to the insertion of the DBS lead for target localization. Neural signals were recorded using a bipolar microelectrode (MicroTargeting Electrode; FHC, Bowdin, ME) advanced during surgery using a microdrive (MicroTargeting Controller; FHC, Bowdin, ME). The initial position of the microelectrode was set to 15mm above the planned target. The microelectrode was advanced in 0.5mm steps and held for 8 seconds to record extracellular signals and local field potential signals. MER signals were amplified with a gain between 100-1000 (D360 Isolated Patient Amplifier System; Digitimer Inc, Hertfordshire, England) and recorded to a computer with custom software (LabView 10.1; National Instruments, Austin, TX) using a USB data acquisition card (Model DT9837A; Data Translations Inc, Marlboro, MA). The hold time for MER recordings at each step was selected to maximize recorded HFB and LFP signals while minimizing overall surgical procedure duration. Step sizes were shortened to 0.1-0.4mm when in the proximity of the STN. The STN dorsal and ventral borders were identified by an electrophysiologist. DBS leads were placed under fluoroscopic visualization with the tip of the DBS lead located near the ventral border of the electrophysiological STN. A movement disorders neurologist activated the DBS electrodes intraoperatively and evaluated the patient for symptom improvements and side effects. After several weeks, allowing intracranial air to resolve, a high-resolution postoperative computed tomography (CT) scan was performed to visualize the location of the DBS leads within the brain.

Local Field Potential Processing

Microelectrode LFP recordings from 2mm above the DB-STN to the ventral border were bandpass filtered between 1Hz to 250Hz and downsampled to a sampling frequency of 500 Hz. The beta frequency band used in this study ranged between 13Hz – 30Hz. Beta power at each

step was calculated by averaging the sum of the squared amplitudes of the Fast Fourier Transform (FFT) at each recording step (Matlab 2012b; The Math Works, Inc., Natick, MA). The FFT included only the first 8 seconds of recorded beta LFP with the first second omitted from analysis to prevent motor noise from the microdrive corrupting the analysis. Histograms were created using each recorded depth average power and a curve was fitted to the resulting plot for figures. Noise from the microdrive or other periods of high electrical noise artifacts observed in the recorded LFP signal were removed from analysis. In this study, we observed noise artifacts to be greater than 3mV and therefore selected this as our threshold for noise detection. Recording depths were normalized to the top of the electrophysiological STN in each trajectory, where 0 mm was the DB-STN. Beta power and contact sites were referenced as a distance away from the DB-STN, 0 mm. The dorsal region was considered to be 0 - 50% of the traversed STN in each trajectory. The ventral region of the STN was considered to be 51-100%.

Image Analysis

Details of the 3-T MR and CT imaging protocols used in this study are described in Patil et al.³³ Briefly, trajectory coordinates for DBS lead locations were identified from postoperative CT scans coregistered to 3-T MRI using a mutual-information algorithm (Analyze 9.0). Spatial locations of active contacts on DBS leads were calculated from the midpoint of the distal most contact (Contact 0) on the visualized DBS lead from coregistered CT images. We used DBS leads with 1.5 mm contact lengths and 0.5 mm spacing between contacts (Model 3889, Medtronic; Minneapolis, MN). The active contact for each trajectory was recorded for each patient during a 6-month postoperative programming session. The optimal contact was selected independent of DB-STN location or peak beta location and was based on clinical benefit evaluated by a neurologist.

The dimensions of the STN (anterior-posterior, medial-lateral) used for midpoint analysis were measured from coronal slices. Figure 4.1 illustrates the method used in this study to identify the midpoint, using a theoretical model of the STN. The most anterior and posterior points of the visualized STN were averaged to determine the midpoint of the STN to define medial and lateral regions. The most medial and lateral points of the visualized STN were used to find the midpoint of the STN defining the anterior and posterior regions. Trajectories were spatially categorized based on the location of the DB-STN relative to the STN midpoint. In our

study, all but four trajectories were categorized as posterior to the STN midpoint. These four trajectories were not included in the analysis of medial and lateral trajectories.

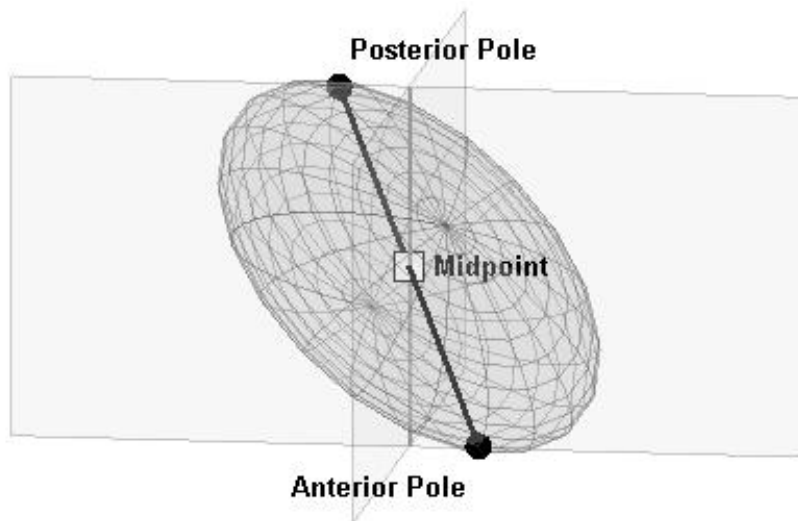


Figure 4.1: STN midpoint analysis on a three dimensional STN model. The anterior and posterior poles are shown through an angled coronal view. Perpendicular planes are drawn through the midpoint to illustrate the sagittal and coronal axes.

Statistical Analysis

Statistical analysis was performed with commercially available software (Matlab 2012b; The Math Works, Inc., Natick, MA, Excel; Microsoft Inc, Redmond, Washington). Distances between optimal contact, peak beta power, DB-STN, and VB-STN are reported in millimeters. Results are expressed as mean \pm SD unless otherwise noted. To compare strength of linear dependence between peak beta power and optimal contact sites, we used the Pearson product-moment correlation coefficient R . Significance was calculated with a significance level of .05 using paired two tailed t-tests.

Results

A total of 26 STN targeted trajectories with recorded LFP signals from 13 PD patients were available for analysis. Of these, 19 trajectories had usable beta LFP signals from which 391 beta power sites were analyzed. Four trajectories were excluded for being categorized as anterior to the STN midpoint. The remaining excluded trajectories had large intermittent noise

artifacts throughout the recorded LFP signal due to technical complications within the surgical setup during MER.

The mean dorsoventral length of recorded STN was 4.0 ± 0.58 mm. There was not a significant difference between the electrophysiologically defined length of the STN and the MRI visualized length of the STN (4.30 ± 1.13 mm, $P = .38$). There also was not a significant difference in the location of the DB-STN relative to the planned target for the electrophysiologically defined STN (13.90 ± 1.20 mm) and the visualized DB-STN (13.97 ± 2.7 mm, $P = .93$).

Beta LFP Peak Power Location Varies Dorsoventrally Through STN

Figure 4.2 displays varying locations of peak beta power with respect to the STN in two sample trajectory recordings. Figure 4.2A shows the peak beta power occurring before the dorsal border of the STN, similar to recent studies.^{13, 19, 20, 22} Conversely, Figure 4.2B shows the peak beta power occurring more centrally within the STN, also similar to previous results.²³ Of the available beta LFP trajectories in this study, 79% had beta peaks in or above the dorsal region of the STN (1.06 ± 0.69 mm). Of these trajectories, 42% had beta peaks above the DB-STN (0.89 ± 0.67 mm). There was a significant correlation between beta peak locations and the DB-STN, $R = .47$, $P = .03$ as illustrated in Figure 4.3A.

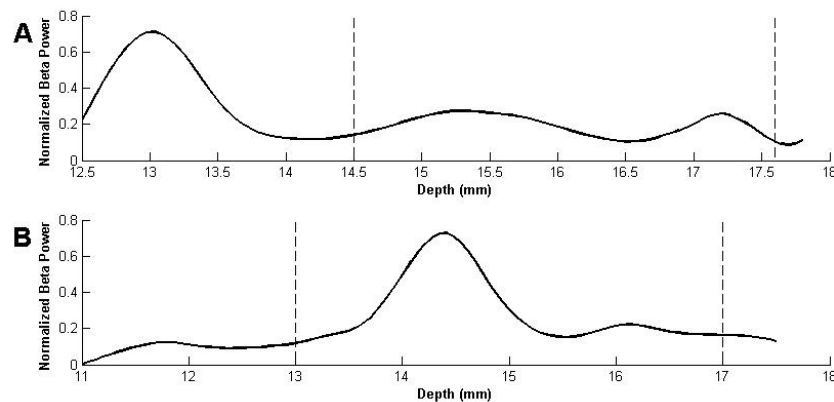


Figure 4.2: Trajectories of beta power through the STN. STN dorsal and ventral boundaries marked with dotted lines. A) Individual beta power trajectory with normalized peak beta power (13.0 mm) occurring before the DB-STN (14.5 mm). B) Individual beta power trajectory with normalized peak beta power (14.4 mm) occurring within marked STN (13 mm – 17mm).

Optimal Contact Location Varies Minimally from STN Dorsal Border

Optimal contact locations varied minimally along the dorsoventral length of the STN from 2mm dorsal to the DB-STN to within the dorsal region of the STN. Of the available trajectories, 63% of trajectories had optimal contacts within or above the dorsal region of the STN (1.0 ± 0.74 mm), with 42% of active optimal contacts above the DB-STN (0.98 ± 0.86 mm). Figure 4.3B shows a significant correlation between optimal contact location and the DB-STN, $R = .42$, $P = .05$. There was a weaker correlation between peak beta locations and optimal contact sites as seen in Figure 4.3C, $R = .37$, $P = .08$.

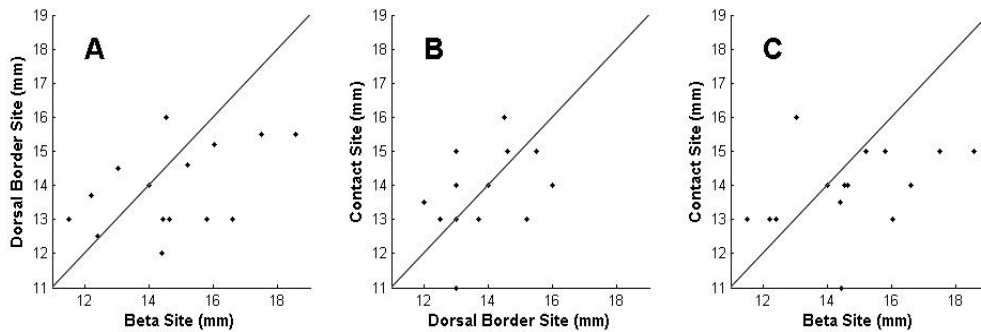


Figure 4.3: Correlation plots for optimal contact locations, peak beta power sites, and the DB-STN for all recorded trajectories. Beta trajectories ranged between 11 mm to 19mm of total recorded track (0 mm to 21mm) A) The correlation between the DB-STN and the peak beta site within each trajectory. B) The correlation between optimal contact site and the DB-STN for all beta trajectories. C) The correlation between all contact sites and peak beta locations.

Variations in Peak Beta and Optimal Contact Sites Explained by Trajectory Location Relative to Visualized STN Midpoint

Figure 4.4 displays the representative average trajectories in this study conditioned on locations relative to STN midpoints. 47% of trajectories were recorded medial of the STN midpoint, while 53% were lateral.

Within the medial trajectory group, the optimal contact location was only slightly below but not significantly different from the peak beta power site (-0.36 ± 1.6 mm, $P = .57$). The optimal contact site was also slightly below but not significantly different from the DB-STN (-0.4 ± 0.94 mm, $P = .30$). The peak beta power location was not significantly different from the DB-STN (-0.04 ± 1.6 mm, $P = .95$).

Within the lateral trajectory group, the optimal contact site was significantly above the peak beta location (1.86 ± 1.32 mm, $P = .002$). The peak beta location was significantly below the DB-

STN (-1.51 ± 1.48 mm, $P = .012$). The DB-STN was not significantly different from the optimal contact site (0.35 ± 1.43 mm, $P = .51$). In all observed trajectories, the optimal contact locations and all but one peak beta sites were above the visualized STN midpoint.

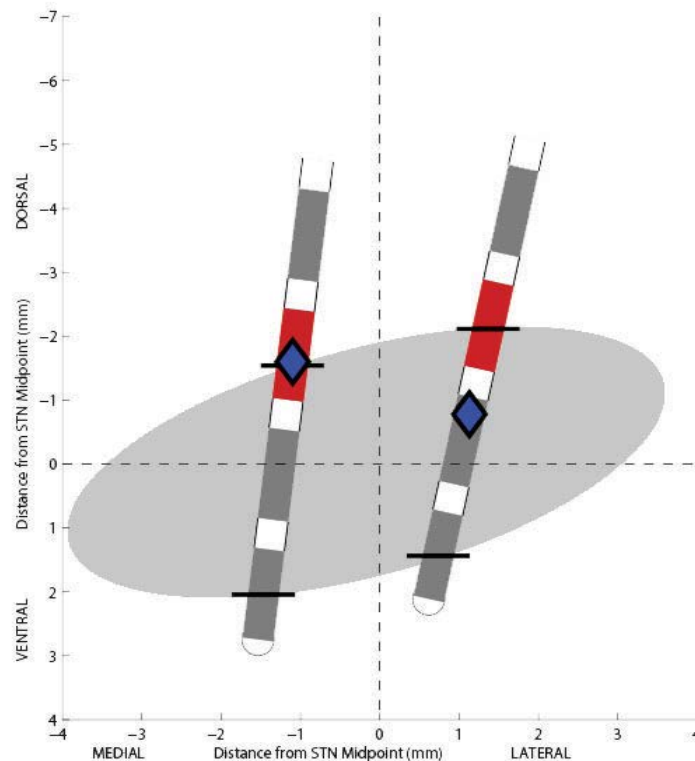


Figure 4.4: Averaged group for medial and lateral trajectories through the STN. A coronal projection of the left STN is shown with black horizontal bars marking the DB-STN and VB-STN for each trajectory. The STN midpoint is centered at (0,0). Illustrated contacts of DBS lead are shown in grey with the optimal contact for stimulation in red. The sites of average peak beta power are shown as blue diamonds along each trajectory.

Discussion

In this study, we examined the relationship between the optimal contacts used in DBS for the treatment of Parkinson's disease with the location of peak beta power recorded during MER. We recorded LFP activity from microelectrodes targeted for the STN and visualized the STN midpoint using high resolution MR imaging (3T). We determined whether the location of peak beta power is correlated to the site of optimal stimulation. These results suggest that the optimal contact location for chronic DBS is associated with peak beta power when implanted trajectories

are medial of the STN midpoint. There was no significant difference between the locations of peak beta power, DB-STN, and optimal contacts for medial trajectories. The optimal contact and peak beta sites were at or near the DB-STN for medial trajectories. However, in trajectories that were lateral of the STN midpoint, the peak beta location was significantly below the active contact and DB-STN. There was no significant difference between the optimal contact site and the DB-STN for lateral trajectories.

The optimal location for stimulation from DBS leads has been a highly debated. Recent studies have found the most optimal location for stimulation to be at or above the DB-STN.^{18, 24, 25} While other studies have claimed the optimal location for stimulation is associated with the location of peak beta power.^{13, 19, 20, 22} Additionally, peak beta power has been shown to occur in the sensorimotor region of the STN, generally observed as the dorsal region of the STN.^{9, 13-17} However, Solages et al found that peak beta power occurred more central in the STN.²³

We applied similar methods of analysis, as in related studies, to the beta-band of LFP signals recorded during MER for each trajectory. Initially, we found that overall beta correlated well with the DB-STN but less so with the optimal contact location. A closer inspection of each trajectory revealed similar results to the differing observations of that found by Zaidel et al and Sloages et al.^{13, 23} Some trajectories in our study had sites of peak beta power dorsal to the DB-STN, whereas others had peak beta sites within the central region of the STN. The optimal contact location did not vary much from the DB-STN region. In order to determine if spatial location relative to the STN affected optimal contact sites we categorized each trajectory based on its location relative to the visualized STN midpoint. Unlike previously reported studies, we used high resolution MR imaging (3T) to directly visualize the STN to identify the STN midpoint and locate each LFP trajectory relative to the visualized midpoint.

We found a fairly equal distribution of trajectories that were medial and lateral of the STN midpoint in the posterior region. Trajectories that were more medial of the STN midpoint had beta peaks and optimal contacts near the DB-STN. This category of trajectories confirms previous findings of optimal contact sites correlated with peak beta hypersynchrony as well as the DB-STN.²⁴ Conversely, trajectories that were more lateral of the STN midpoint had peak beta sites significantly ventral of the optimal contact site and DB-STN. There was no significant difference between the optimal contact location and the DB-STN for lateral trajectories. On

average, we did confirm peak beta power locations to be in the dorsal region of the STN. However, sites of optimal contact were significantly more dorsal to these peak beta locations. This result may be limited by our selection of the midpoint of the optimal contact to calculate significance. In our study, DBS lead contacts were 1.5mm in length and selection of a point in the contact closer to peak beta hypersynchrony may provide improved correlations. However, unlike previous studies, we had significantly better resolution during MER recordings and therefore were more precise with the location of peak beta relative to the optimal contact. It should be noted, on average the active contact was either the nearest point of stimulation or the contact just dorsal to the peak beta point for lateral trajectories.

Interestingly, we found optimal contacts to be significantly ventral of peak beta sites for the four trajectories excluded from our analysis for being anterior of the STN midpoint (-2.27 ± 1.39 mm, $P = .02$). We observed no significant difference between the peak beta site and the DB-STN of these lateral-anterior trajectories (-0.3 ± 1.1 mm, $P = .33$). This result may be explained by the dorsal lateral posterior region of the STN being the most therapeutically beneficial site for DBS stimulation. The optimal contact of these anterior trajectories was the closest contact to the lateral posterior region of the STN.

We present a potential explanation for the differences in recently published results indicating optimal contact locations for STN DBS by precisely locating recorded trajectories relative to the STN using high resolution MRI. By direct visualization of the STN we were able to determine the location of each of our MER LFP trajectories relative to the individually visualized STN midpoints. We have shown that differences in optimal contact and peak beta locations may be dependent on the relative location of the recorded trajectory to the STN midpoint. Beta oscillatory activity may vary significantly depending on region of STN traversed. We found that trajectories medial of the STN midpoint had optimal contacts that were significantly correlated to the beta-LFP peak power location and the DB-STN. We found trajectories lateral of the STN midpoint to have optimal contacts that were significantly correlated with the DB-STN but not with peak beta power sites; which were significantly ventral of the DB-STN. These results may have further implications in studies modeling STN beta oscillations, post-operative DBS parameter selections, and closed-loop stimulation technologies.

References

1. Benabid AL, Chabardes S, Mitrofanis J, Pollak P. Deep brain stimulation of the subthalamic nucleus for the treatment of Parkinson's disease. *Lancet Neurol*. 2009 Jan;8(1):67-81.
2. Krack P, Pollak P, Limousin P, Benazzouz A, Benabid AL. Stimulation of subthalamic nucleus alleviates tremor in Parkinson's disease. *The Lancet*. 1997;350(9092):1675.
3. Kumar R, Lozano AM, Kim YJ, et al. Double-blind evaluation of subthalamic nucleus deep brain stimulation in advanced Parkinson's disease. *Neurology*. 1998;51(3):850-5.
4. Liang GS, Chou KL, Baltuch GH, et al. Long-term outcomes of bilateral subthalamic nucleus stimulation in patients with advanced Parkinson's disease. *Stereotact Funct Neurosurg*. 2006;84(5-6):221-7.
5. Lang AE. Surgery for Parkinson disease: A critical evaluation of the state of the art. *Arch Neurol*. 2000 Aug;57(8):1118-25.
6. Rodriguez-Oroz MC, Zamarbide I, Guridi J, Palmero MR, Obeso JA. Efficacy of deep brain stimulation of the subthalamic nucleus in Parkinson's disease 4 years after surgery: double blind and open label evaluation. *J Neurol Neurosurg Psychiatry*. 2004 Oct;75(10):1382-5.
7. Benabid AL, Pollak P, Gross C, et al. Acute and long-term effects of subthalamic nucleus stimulation in Parkinson's disease. *Stereotact Funct Neurosurg*. 1994;62(1-4):76-84.
8. Krack P, Benazzouz A, Pollak P, et al. Treatment of tremor in Parkinson's disease by subthalamic nucleus stimulation. *Mov Disord*. 1998 Nov;13(6):907-14.
9. Kuhn AA, Trottenberg T, Kivi A, Kupsch A, Schneider GH, Brown P. The relationship between local field potential and neuronal discharge in the subthalamic nucleus of patients with Parkinson's disease. *Exp Neurol*. 2005 Jul;194(1):212-20.
10. Bronte-Stewart H, Barberini C, Koop MM, Hill BC, Henderson JM, Wingeier B. The STN beta-band profile in Parkinson's disease is stationary and shows prolonged attenuation after deep brain stimulation. *Exp Neurol*. 2009 Jan;215(1):20-8.
11. Brown P, Williams D. Basal ganglia local field potential activity: character and functional significance in the human. *Clin Neurophysiol*. 2005 Nov;116(11):2510-9.
12. Ray NJ, Jenkinson N, Wang S, et al. Local field potential beta activity in the subthalamic nucleus of patients with Parkinson's disease is associated with improvements in bradykinesia after dopamine and deep brain stimulation. *Exp Neurol*. 2008 Sep;213(1):108-13.
13. Zaidel A, Spivak A, Grieb B, Bergman H, Israel Z. Subthalamic span of beta oscillations predicts deep brain stimulation efficacy for patients with Parkinson's disease. *Brain*. 2010 Jul;133(Pt 7):2007-21.
14. Zaidel A, Spivak A, Shpigelman L, Bergman H, Israel Z. Delimiting subterritories of the human subthalamic nucleus by means of microelectrode recordings and a Hidden Markov Model. *Mov Disord*. 2009 Sep 15;24(12):1785-93.
15. Trottenberg T, Kupsch A, Schneider GH, Brown P, Kuhn AA. Frequency-dependent distribution of local field potential activity within the subthalamic nucleus in Parkinson's disease. *Exp Neurol*. 2007 May;205(1):287-91.

16. Weinberger M, Mahant N, Hutchison WD, et al. Beta oscillatory activity in the subthalamic nucleus and its relation to dopaminergic response in Parkinson's disease. *J Neurophysiol.* 2006 Dec;96(6):3248-56.
17. Chen CC, Pogosyan A, Zrinzo LU, et al. Intra-operative recordings of local field potentials can help localize the subthalamic nucleus in Parkinson's disease surgery. *Exp Neurol.* 2006 Mar;198(1):214-21.
18. Whitmer D, de Solages C, Hill B, Yu H, Henderson JM, Bronte-Stewart H. High frequency deep brain stimulation attenuates subthalamic and cortical rhythms in Parkinson's disease. *Front Hum Neurosci.* 2012;6:155.
19. Ince NF, Gupte A, Wichmann T, et al. Selection of optimal programming contacts based on local field potential recordings from subthalamic nucleus in patients with Parkinson's disease. *Neurosurgery.* 2010 Aug;67(2):390-7.
20. Yoshida F, Martinez-Torres I, Pogosyan A, et al. Value of subthalamic nucleus local field potentials recordings in predicting stimulation parameters for deep brain stimulation in Parkinson's disease. *J Neurol Neurosurg Psychiatry.* 2010 Aug;81(8):885-9.
21. Pogosyan A, Yoshida F, Chen CC, et al. Parkinsonian impairment correlates with spatially extensive subthalamic oscillatory synchronization. *Neuroscience.* 2010 Nov 24;171(1):245-57.
22. Abosch A, Lanctin D, Onaran I, Eberly L, Spaniol M, Ince NF. Long-term recordings of local field potentials from implanted deep brain stimulation electrodes. *Neurosurgery.* 2012 Oct;71(4):804-14.
23. de Solages C, Hill BC, Yu H, Henderson JM, Bronte-Stewart H. Maximal subthalamic beta hypersynchrony of the local field potential in Parkinson's disease is located in the central region of the nucleus. *J Neurol Neurosurg Psychiatry.* 2011 Dec;82(12):1387-9.
24. Godinho F, Thobois S, Magnin M, et al. Subthalamic nucleus stimulation in Parkinson's disease : anatomical and electrophysiological localization of active contacts. *J Neurol.* 2006 Oct;253(10):1347-55.
25. Saint-Cyr JA, Hoque T, Pereira LC, et al. Localization of clinically effective stimulating electrodes in the human subthalamic nucleus on magnetic resonance imaging. *J Neurosurg.* 2002 Nov;97(5):1152-66.
26. Sterio D, Zonenshayn M, Mogilner AY, et al. Neurophysiological refinement of subthalamic nucleus targeting. *Neurosurgery.* 2002 Jan;50(1):58-67; discussion -9.
27. Starr PA, Christine CW, Theodosopoulos PV, et al. Implantation of deep brain stimulators into the subthalamic nucleus: technical approach and magnetic resonance imaging-verified lead locations. *J Neurosurg.* 2002 Aug;97(2):370-87.
28. Holloway KL, Gaede SE, Starr PA, Rosenow JM, Ramakrishnan V, Henderson JM. Frameless stereotaxy using bone fiducial markers for deep brain stimulation. *J Neurosurg.* 2005 Sep;103(3):404-13.
29. Bejjani BP, Dormont D, Pidoux B, et al. Bilateral subthalamic stimulation for Parkinson's disease by using three-dimensional stereotactic magnetic resonance imaging and electrophysiological guidance. *J Neurosurg.* 2000 Apr;92(4):615-25.
30. Hutchison WD, Allan RJ, Opitz H, et al. Neurophysiological identification of the subthalamic nucleus in surgery for Parkinson's disease. *Ann Neurol.* 1998 Oct;44(4):622-8.

31. Gross RE, Krack P, Rodriguez-Oroz MC, Rezaei AR, Benabid AL. Electrophysiological mapping for the implantation of deep brain stimulators for Parkinson's disease and tremor. *Mov Disord.* 2006 Jun;21 Suppl 14:S259-83.
32. Hamani C, Richter EO, Andrade-Souza Y, Hutchison W, Saint-Cyr JA, Lozano AM. Correspondence of microelectrode mapping with magnetic resonance imaging for subthalamic nucleus procedures. *Surg Neurol.* 2005 Mar;63(3):249-53; discussion 53.
33. Patil PG, Conrad EC, Aldridge JW, Chenevert TL, Chou KL. The anatomical and electrophysiological subthalamic nucleus visualized by 3-T magnetic resonance imaging. *Neurosurgery.* 2012 Dec;71(6):1089-95; discussion 95.
34. Coste J, Ouchchane L, Sarry L, et al. New electrophysiological mapping combined with MRI in parkinsonian's subthalamic region. *Eur J Neurosci.* 2009 Apr;29(8):1627-33.

Chapter 5 : Activation of Subthalamic Nucleus in Local Field Potentials and Single Units during Response Inhibition

Abstract

Background: Activation of the subthalamic nucleus (STN) during response inhibition is important for understanding basal ganglia circuitry and motor decision connections in the brain.

Objectives: The goal of this study was to record local field potential (LFP) and single unit activity (SUA) from the STN intraoperatively during a stop-signal task. We analyzed the activation of the theta, alpha, and beta bands of the LFP and the firing frequency modulations of single units in order to confirm previously reported results of STN activation during response inhibition.

Methods: We collected LFP and SUA from wideband recordings using microelectrodes in the STN of 3 patients undergoing deep brain stimulation (DBS) surgery for Parkinson's disease. Patients completed a stop-signal task while a microelectrode was held in a fixed location within the STN. The task was analyzed on triggers for movement cue, movement onset, and the stop-signal cue. We compared STN activation in trials for successful and unsuccessful movement inhibition and trials without stop-signals.

Results: We found significant increases in the theta and alpha bands in the presence of the stop-signal and movement onset ($P = .002$, $P < .001$, $P = .002$). We observed decreases in beta power for unsuccessful response inhibition compared to successful inhibition. SUA also showed decreases in firing frequency on the stop signal for failed inhibition versus success. Generally we observed single units to be movement responsive indicating recording locations to be in the sensorimotor region of the STN.

Conclusion: We confirm recent studies reporting variations in the theta, alpha, and beta bands of the STN during response inhibition and movement. We can corroborate the significant

difference seen in beta power of the STN between failed and successful response inhibition. These results provide further evidence that the STN is considered the “brake” for planned actions and operates by regulating inhibitory signals seen clearly in the beta LFP.

Introduction

Deep brain stimulation (DBS) of the subthalamic nucleus (STN) is an effective treatment for the motor symptoms of Parkinson disease (PD). The STN is considered to play a major role in motor control by influencing the basal ganglia through inhibitory signals.¹ Specifically, the STN is thought to regulate the inhibition of planned and initiated movements.

Recent studies using functional magnetic resonance imaging (fMRI) reported increased BOLD signal response in the STN during movement inhibition for patients performing a stop-signal task.²⁻⁶ The stop-signal task was designed to isolate and assess the neural network responsible for sudden cancellation of an intended or in-progress action.⁷ Although many variations exist, the paradigm generally prompts subjects to respond in the direction of an on-screen cue either through a button press or rotation of a joystick. Intermittently throughout the task, a stop cue is presented and the subject is instructed to refrain from response. The stop signal is varied to prevent subjects from anticipating the cue and is typically designed to elicit successful response inhibition in half of all stop-signal trials.

Studies using the stop-signal task and recordings from within the STN have also shown significant activation of the STN during movement inhibition in local field potentials (LFP).^{1,6} The power of the LFP beta band was observed to significantly decrease prior to and during movement. Beta power has also been reported to reduce significantly with dopamine replacement medication and DBS.⁸⁻¹³ The theta band has also been reported to show significant increases during inhibition signals in stop-signal tasks.⁶

Here we investigate the implication of the beta, theta and alpha bands in the LFP as well as single units in the inhibitory role of the STN. We intraoperatively recorded LFPs and SUA from within the STN of PD patients during a stop-signal task using microelectrode recording (MER) probes. We confirmed previously reported findings of distinct patterns of STN activity in different LFP frequency bands associated with successful and unsuccessful inhibition to movement. We also observed movement responsive units providing evidence of task recordings within the motor region of the STN. We provide supporting evidence of STN involvement in response inhibition.

Methods

Patient Selection

We studied 3 consecutive patients with advanced idiopathic Parkinson disease who underwent STN DBS surgery at our institution (3 men; age, 66 ± 6 years; range, 52-73 years). Patient selection criteria for DBS has been previously described in Patil et al.¹⁴ Briefly, selected patients were diagnosed with Parkinson disease and had motor fluctuations not well controlled by medications or had levodopa-unresponsive tremor. Patients were excluded from this study if abnormalities in brain anatomy existed or intraoperative fatigue prevented completion of the task. Patients were introduced to the stop-signal task two weeks prior to surgery in a preoperative clinical visit. In this study, only intraoperative off-medication patient data is presented. We performed the study in accordance with the policies of the Medical Institutional Review Board of the University of Michigan.

DBS Procedure

The DBS procedure used in this study has previously been described.¹⁴ Briefly, all patients underwent 3-T MRI using a coronal imaging protocol designed for visualization of the STN. Patients were fitted with a Leksell stereotactic frame (Elekta Instruments AB, Stockholm, Sweden) and underwent a preoperative 1.5-T MRI the day of surgery. Both 3-T and 1.5T MR images were coregistered using a mutual-information algorithm (Analyze 9.0; AnalyzeDirect, Inc, Overland Park, Kansas). Frame-based bilateral surgical targeting was then performed with commercial software (Framelink; Medtronic, Inc, Minneapolis, Minnesota). Initial indirect targeting at 12 lateral, 3 posterior, and 4 inferior to the midcommissural point was performed and then fine-tuned to the individual patient according to the MRI-visualized STN.

During surgery, MER was performed prior to the insertion of the DBS lead for target localization. Neural signals were recorded using a bipolar microelectrode (MicroTargeting Electrode; FHC, Bowdin, ME) advanced during surgery using a microdrive (MicroTargeting Controller; FHC, Bowdin, ME). The STN dorsal and ventral borders were identified by an electrophysiologist. Once the MER probe was confirmed within the STN region a location with sustained neuronal firing was found and the stop signal task was performed.

DBS leads were placed under fluoroscopic visualization with the tip of the DBS lead located near the ventral border of the electrophysiological STN. A movement disorders neurologist activated the DBS electrodes intraoperatively and evaluated the patient for symptom improvements and side effects. After several weeks, allowing intracranial air to resolve, a high-resolution postoperative computed tomography (CT) scan was performed to visualize the location of the DBS leads within the brain.

Stop Signal Paradigm

The stop signal task was used to assess motor inhibition response in PD patients during DBS surgery.⁷ The task used in this study is an adaptation of that described in Aron et.al.² Briefly, the stop-signal task enables the examination of neural structures involved in going and stopping motor movement decisions. The paradigm presented patients with choice responses and occasionally presented a stop signal to make patients attempt to inhibit their response. The task was optimized to maximize differences in recorded signals between Stop and Go events by predetermining the sequence of Go and Stop trials. Stop trials were triggered with a Stop-signal delay (SSD); which was dynamically adjusted to yield a 50% successful inhibition rate so that Stop-signal-Reaction-Time (SSRT) could be estimated for each session. The SSRT was calculated by subtracting the SSD from the median reaction time of Go trials.

Specifically for this study, the stop-signal task was presented to patients intraoperatively on a computer display. Patients were given a joystick (Freedom 2.4, Logitech; Round Rock, TX) and instructed to rotate the joystick with the contralateral hand in the direction of the Instruction cue presented on screen. Patients completed at least 4 blocks of trials for each session, with each block consisting of 24 trials of both Go and Stop trials. Each trial in the task started with a Trial Begin cue on a black screen which lasted for 1 second and was followed by the Instruction cue. In this study, Instruction cues were presented as white blocks filling half the screen; indicating direction of rotation while the other half of the screen remained black. Stop signals were flashed in red over white blocks in Stop trials. Trial durations were set to 2 seconds from Trial Begin to Trial End. If the patient completed a Go trial by a full rotation of the joystick within the trial duration, the screen was set to black for the remainder of the trial duration. If the patient failed to complete a Go trial within the trial duration the trial was removed from analysis. In Stop

trials, patients who successfully inhibited response had their screen remain red for the remainder of the trial duration. If inhibition was not successful, the screen was set to black for the remainder of the trial duration. Also, if patients rotated the joystick in the direction opposite of the Instruction cue, that trial was removed from analysis.

Segmentation of Task Data

The recorded electrophysiological data for each session in this study was segmented using three different trigger events. The events triggers included the instruction cue, the initiation of movement, and the stop signal cue. Each event spanned 1 s before the trigger and 1 s after. We grouped the task data into four different types of trials. These trial types were: “No-Stop”, “MaybeStop-Go”, “MaybeStop-Stop-correct”, and “MaybeStop-Stop-fail”.

The task consisted of 20% No-Stop (NS) trials and 80% MaybeStop (MS) trials (Figure 5.1). There were significantly more MS trials than “No-Stop” trials in this task in order to ensure a statistically relevant number of stop signal trials were presented to the patient. Overall, patients were presented with approximately 60% Go trials and 40% Stop trials since MS trials consisted of MS-Go and MS-Stop trials. In “No-Stop” trials, patients were instructed that the stop signal would not appear. However in MS trials, patients were instructed that half of the trials in this type would have the stop signal appear. Within MS trials, 50% of trials were MS-Go and 50% were MS-Stop; in which the stop signal was presented to the patient at some variable SSD. The SSD was dynamically adjusted from 100ms during the session in 50ms steps depending on if inhibition was successful or not. This allowed for approximately equal proportions of MS-Stop-fail and MS-stop-success trials.

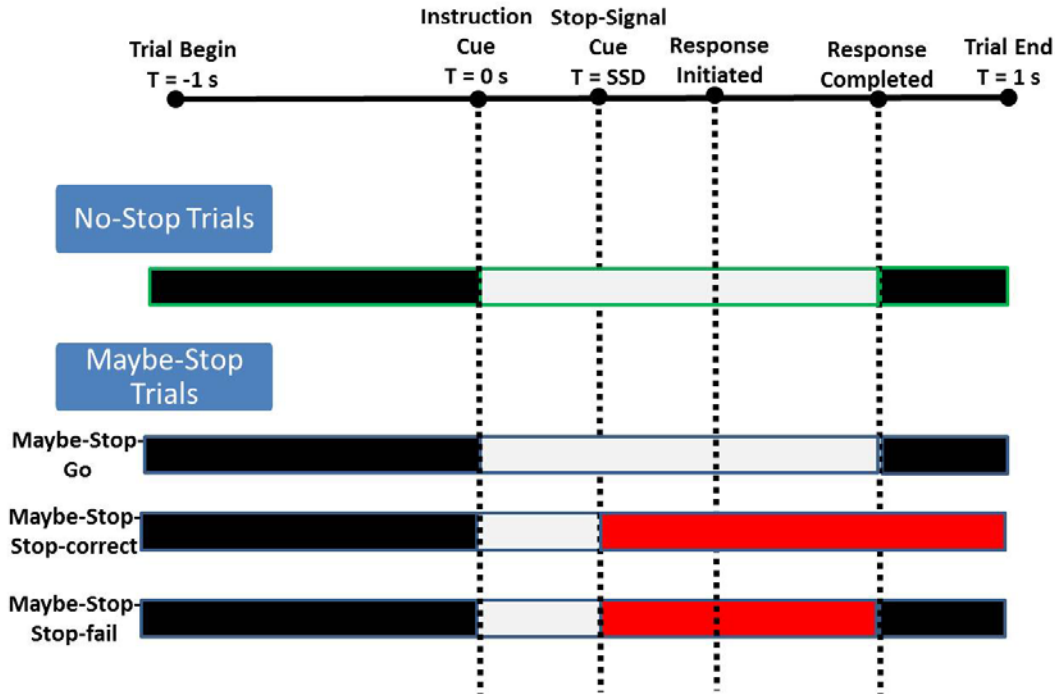


Figure 5.1: Stop-signal paradigm used intraoperatively with PD patients. There were 2 groups of trial types: No-Stop and Maybe-Stop trials. All trials were presented with the trial group printed to screen 1 second prior to the instruction cue indicating either left or right rotation of the joystick for response movement. Initiated movement was recorded between instruction cue and completed response ending the trial. In MaybeStop-Stop trials the stop-signal was flashed on screen at a variable SSD. Successful inhibition of joystick rotation kept the stop cue on screen until trial end. Unsuccessful inhibition was recorded with the initiation of movement after the stop-signal appeared. A blank screen appeared after response completions until the trial ended.

Signal Processing and Statistical Analysis

Wideband data from MER within the STN were recorded for each session in a single continuous file sampled at 30 kHz for each patient (Matlab 2012, Mathworks). Single unit activity (SUA) for each session was bandpass filtered from 500 to 2 kHz. SUA wavelet filtered data was sorted for spikes over the duration of the task recording (Offline Sorter, Plexon; Dallas, TX). Autocorrelograms of spike counts were used to ensure multiple units were not analyzed as one unit and firing frequencies were within physiological bounds. SUA timestamps were synced with movement data and trial events recorded at 30 kHz from an analog joystick and an on screen photodiode (LiCor) respectively.

LFP activity for each session was extracted from wideband data from the single continuous recording for each patient using the procedure described in Leventhal et al.¹⁵ Briefly,

the LFP signal was decimated with a 1000th order finite impulse response anti-aliasing filter and downsampled to 500 Hz. All data from 1 to 100 Hz were included in all analyses.

Gabor power spectrograms were computed to examine spectral power over time by convolving LFPs with Gaussian-tapered complex sinusoids of integer frequencies from 1 to 100 Hz and taking the squared magnitude of the resulting time-series. The logarithms of the spectrograms were then averaged for each recording session.

Continuous measure of the theta, alpha, and beta power bands were calculated by zero-phase-shift filtering of the LFP data between 2 – 6 Hz, 8 – 13 Hz, and 15 – 25 Hz using an FIR filter. The filtered signal was Hilbert transformed to create the analytic signal and the magnitude of the signal was squared to provide a continuous measure of the power in the LFP frequency band of interest.

Significance for individual LFP band power for each session was determined by z-scores. Mean power for each band during trials was obtained by shifting timestamps corresponding to the trial-Begin event forward or backward in time by random interval between -1 and 2 seconds. The shift generated a random sample of local band powers during each trial, which were averaged to yield mean power for each band for a single iteration. This procedure was repeated 10,000 times to generate a distribution of mean powers for each band, from which the mean and standard deviations were calculated.

Comparisons of power z-scores between trial types within a given session and frequency band were calculated using a two-sample paired t-test with a significance level of $p < .001$.

Results

In this study, 3 PD patients undergoing DBS surgery were examined. We simultaneously recorded SUA and LFP signals from 4 STN. Recordings were electrophysiologically confirmed to be with the STN. A total of 527 trials of the stop-signal task were performed with an average of 131 trials per session. The average reaction time (RT) for all sessions was 621.75ms. Table 5.1 shows the count for each trial type and average stop signal reaction time (SSRT) for each session.

	Trials	NS	MSG	MSS-succ.	MSS-fail	SSRT (ms)	Mean RT (ms)	Mean Firing Rate (Hz)
Recording 1	96	16	48	17	4	289	364	24
Recording 2	95	16	47	15	3	287	376	29
Recording 3	144	24	72	28	20	376	610	25
Recording 4	192	32	96	44	17	684	1137	15
Mean	131.75	22	65.75	26	11	409	621.75	23.25

Table 5.1: Counts for each trial type, reaction time, and firing rate for each recording session. SSRT was calculated by subtracting SSD from the median reaction time of “MaybeStop-Go” trials. Reaction times were calculated from instruction cue onset to trial completion.

The average SSRT for “No-Stop” trials in this study was 0.59 seconds while the average for “MaybeStop-Go” trials was 0.68 seconds (Figure 5.2). The fastest SSRT was observed in “MaybeStop-Stop-fail” trials to be 0.46 seconds.

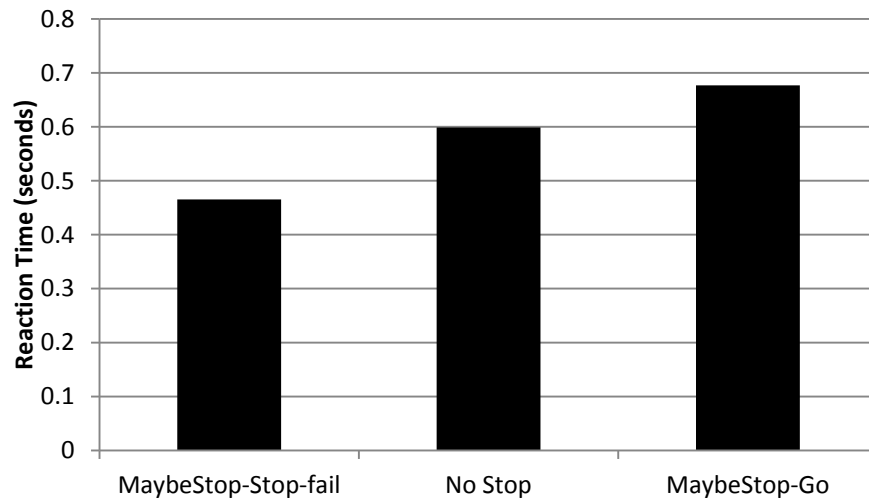


Figure 5.2: Race model reaction times for movement trial types “MaybeStop-Stop-fail”, “No-Stop” and “MaybeStop-Go”.

Theta Band Response

Theta oscillations of the LFP signal increased significantly immediately after movement initiation for all “No-Stop” and “MaybeStop-Stop-fail” trials but not “MaybeStop-Go” trials (Figure 5.3A). Trials of the “No-Stop” type had peak theta activity occur 310 ms after movement was triggered and was significantly greater than “MaybeStop-Go” trials ($P = .005$). The theta band showed significant increases to the presence of the stop signal; which was highest when response inhibition was unsuccessful ($t = 0.44$ s, $P = .002$). A marked increase in theta band activity for “No-Stop” trials was also observed between the instruction cue and movement

initiation ($t = -0.44$ s, $P = .016$) compared to a significant decrease in theta activity for “MaybeStop-Stop-fail” trials prior to the start of movement ($t = -0.48$ s, $P = .014$).

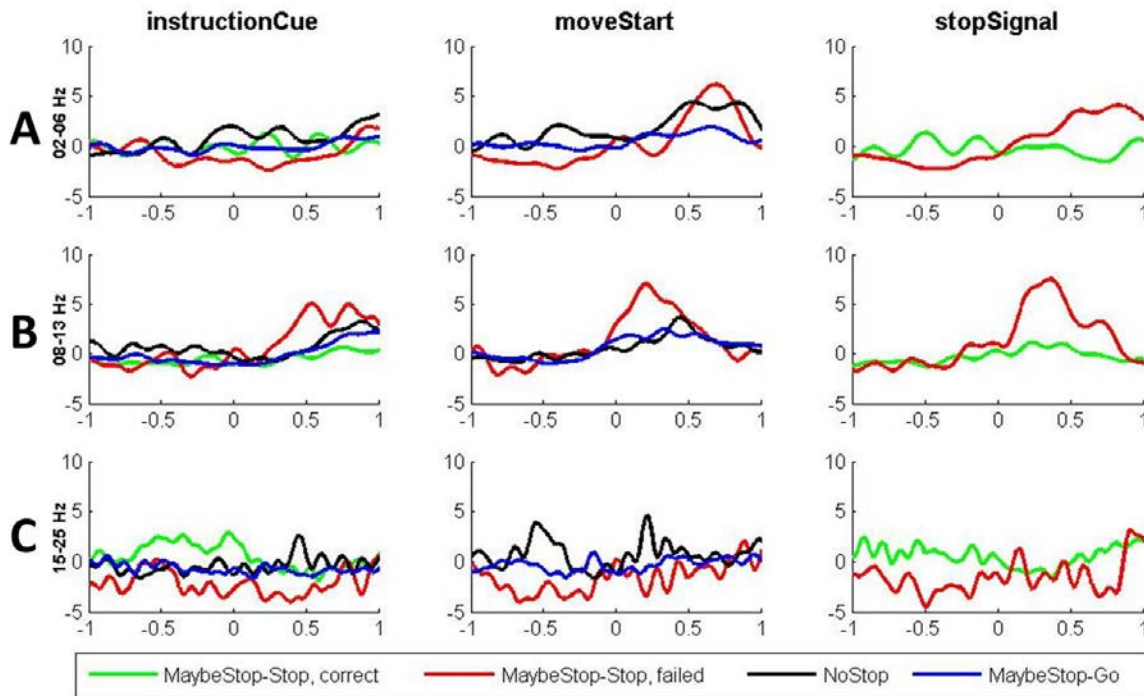


Figure 5.3: Normalized z-score plots for triggered events for theta, alpha, and beta bands. A) Theta LFP response for all trial types. B) Alpha LFP response for all trial types. C) Beta LFP response for all trial types.

Alpha Band Response

Alpha band oscillations were observed to be significantly increased in response to movement for all movement trial types (Figure 5.3B). “No-Stop” trials had greater power increases in the alpha band compared to “MaybeStop-Go” trials, although peak power for the later trial type occurred 70 ms earlier. Trials for unsuccessful response inhibition had a sustained significant increase in the alpha band for a 1 second period starting just before triggered movement with the peak in power 210 ms after movement trigger ($P = .001$). Alpha oscillations also showed a significant increase in “MaybeStop-Stop-fail” trials but not “MaybeStop-Stop-correct” trials to the presence of the stop signal ($P < .001$).

Beta Band Response

The beta band of the recorded LFP signals had significant decreases in activity throughout the duration of the “MaybeStop-Stop-fail” trials starting 400 ms before the instruction cue ($P < .001$) (Figure 5.3C). Conversely, the “MaybeStop-Stop-correct” trials had a significant and sustained increase 500 ms before the instruction cue ($P = .007$). When triggered on movement initiation, “No-Stop” trials had a significant increase in activity 180 ms after the trigger while “MaybeStop-Stop-fail” trials had nearly the exact opposite response in beta power at the same time ($P = .002$). In response to the stop signal, “MaybeStop-Stop-fail” trials continued to have a significant decrease in activity compared to “MaybeStop-Stop-correct” trials ($P < .001$) (Figure 5.4). “MaybeStop-Go” and “No-Stop” trials had similar responses in beta band activity until movement was initiated. After movement, “MaybeStop-Go” continued to have no significant changes in beta response activity throughout the remainder of the trial duration.

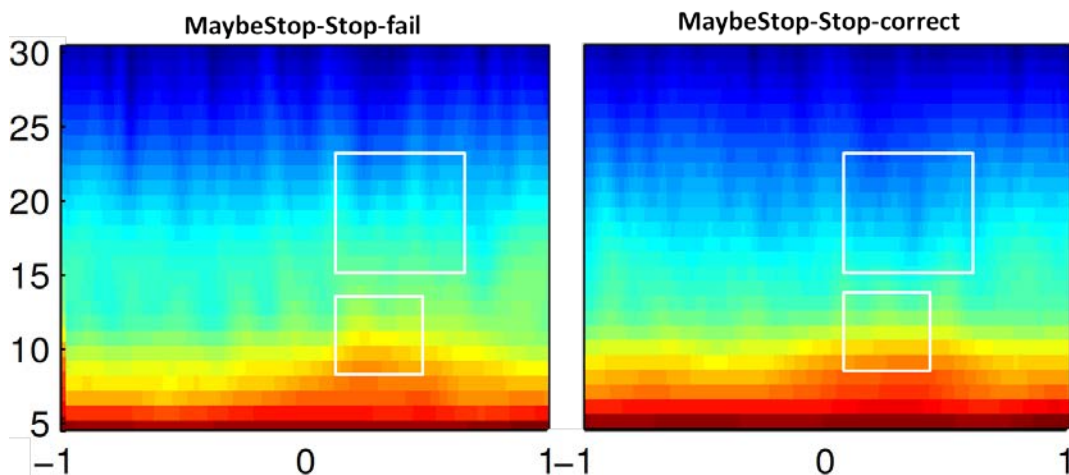


Figure 5.4: Scalogram plots from 5 Hz to 30 Hz for “MaybeStop-Stop-fail” and “MaybeStop-Stop-correct” trial types centered on the Stop-Signal cue. The top white boxes highlight the differences in power in the beta band. The lower boxes show the differences in power between successful and unsuccessful response inhibition in the alpha band.

Single Unit Response

Single unit activity recorded simultaneously with LFP showed similar changes in firing frequency to LFP power in the beta band for response to stop signal inhibition. Firing frequency on average was significantly lower for “MaybeStop-Stop-fail” trials compared to “MaybeStop-Stop-correct” trials ($P < .001$) in the presence of the stop-signal (Figure 5.5). There was a marked increase in firing frequency in response to movement for both “No-Stop” and

“MaybeStop-Go” trials just after the trigger. Although the “No-Stop” trials had a slightly larger and earlier increase in firing rate ($t = 0.14$ s, $f = 29$ Hz, $P < .001$). The “MaybeStop-Stop-fail” trials had an increase in firing rate just before the triggered movement and a firing rate larger than both “MaybeStop-Go” and “No-Stop” trials ($t = -0.04$, $f = 30.79$ Hz, $P < .001$). Overall, firing rates for the “MaybeStop-Stop-fail” trials were significantly slower than the other trial types ($P < .001$).

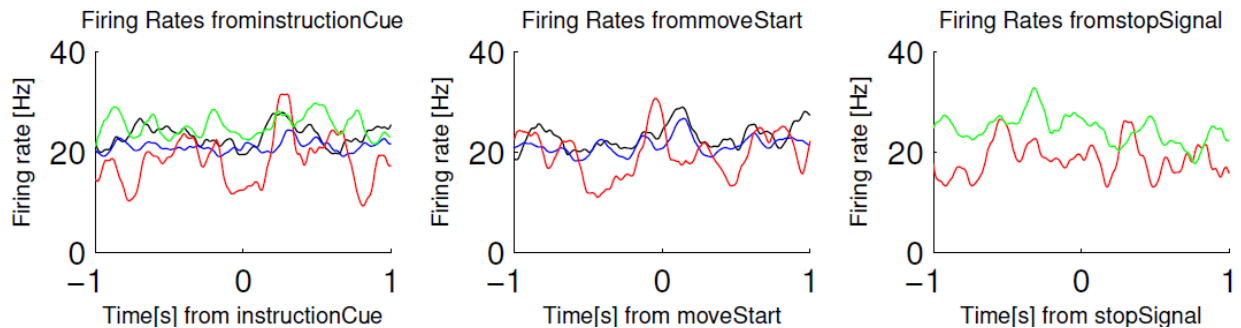


Figure 5.5: Average firing rate for the recorded single units across the three trigger events. The trial types are represented by different colors, Black (“No-Stop”), Blue (“MaybeStop-Go”), Red (“MaybeStop-Stop-fail”), Green (“MaybeStop-Stop-correct”).

Discussion

In this study we confirmed previous findings of the role the STN has in response inhibition through the analysis of three main LFP frequency bands and SUA. We recorded SUA and LFP activity simultaneously with microelectrodes in the STN during DBS surgery for Parkinson’s disease. We correlated electrophysiological STN activity with an adapted stop-signal task performed by patients intraoperatively. We confirmed the significance of the STN in successful inhibition to movement by analyzing the theta, alpha, and beta bands of LFP and the changes in firing frequency of movement responsive neurons.

We found that the STN had significant decreases in beta power and single unit firing frequencies in unsuccessfully inhibited movement trials compared to successful response inhibition in the presence of a stop signal. This is consistent with recent studies identifying the STN as the primary “brake” in the basal ganglia; using inhibitory signals to regulate responses.^{2, 4, 5, 16-20} Decreases in firing frequency and beta power triggered on the stop signal may suggest the failure of the STN to respond in time to inhibit movement. Conversely, we did not observe

any changes in beta power after the instruction cue for successfully inhibited response trials. This may suggest that the inability of the beta band to return to baseline in failed inhibition trials is the result of an already programmed action for movement unable to be cancelled. The beta band may control the cancellation of movement by maintaining a threshold of activity level as suggested in recent studies.^{1, 9, 21-24} These results further add to the role of the beta band in preparation and execution of movement.

Theta activity appeared to be related to movement trials in the stop-signal task of our study. We observed an increase in activity for “No-Stop” and “MaybeStop-Stop-fail” trials triggered on movement initiation. There was a significant difference in activity between the failed and successful response inhibition trials in the presence of the stop signal. We confirmed that increases in theta STN activity were related to decision and movement cues described in recent studies using inhibitory tasks.^{6, 25, 26}

We did not observe any significant variations in the alpha band to the instruction cue for any trial types in this study. There were increases in power related to movement for all response type trials as well as a significant increase of failed inhibition trials compared to successful stops.

In our limited patient population, we did confirm that the race condition described by Logan and Cowan was met.⁷ As expected, the reaction times for failed stop trials were shorter than “No-Stop” trials which were shorter than the slowest reaction times of “MaybeStop-Go” trials. However, since the average reaction time for our patient population was considerably longer than that of normal subjects performing the stop-signal task; we cannot definitively confirm the electrophysiological characteristics of the STN in inhibitory control. Additionally in this study, we were constrained to using microelectrodes for recording electrophysiological data from within the STN. Most recent studies have used DBS leads either intraoperatively or postoperatively externalized for performing stop-signal tasks with patients. This enables the capability to record from multiple locations within the STN region, including the sensorimotor area, simultaneously in order to identify potential sites that may be task responsive. We were limited to selected sites in the STN without the ability to discern the most optimal area for task responsiveness.

Our findings provide further direct evidence and confirmation of the engagement of the STN in a task requiring movement inhibition. The involvement and modulation of STN neuronal activity during response inhibition is evident in the main frequency bands of the LFP as well as single unit recordings from within the region. These results from patients with PD should be interpreted cautiously as the correlation with normal physiological conditions is uncertain.

References

1. Kuhn AA, Trottenberg T, Kivi A, Kupsch A, Schneider GH, Brown P. The relationship between local field potential and neuronal discharge in the subthalamic nucleus of patients with Parkinson's disease. *Exp Neurol*. Jul 2005;194(1):212-220.
2. Aron AR. Cortical and Subcortical Contributions to Stop Signal Response Inhibition: Role of the Subthalamic Nucleus. *Journal of Neuroscience*. 2006;26(9):2424-2433.
3. Chambers JM, Prescott TJ. Response times for visually guided saccades in persons with Parkinson's disease: a meta-analytic review. *Neuropsychologia*. Mar 2010;48(4):887-899.
4. Frank MJ. Hold your horses: a dynamic computational role for the subthalamic nucleus in decision making. *Neural Netw*. Oct 2006;19(8):1120-1136.
5. Eagle DM, Baunez C, Hutcheson DM, Lehmann O, Shah AP, Robbins TW. Stop-signal reaction-time task performance: role of prefrontal cortex and subthalamic nucleus. *Cereb Cortex*. Jan 2008;18(1):178-188.
6. Alegre M, Lopez-Azcarate J, Obeso I, et al. The subthalamic nucleus is involved in successful inhibition in the stop-signal task: a local field potential study in Parkinson's disease. *Exp Neurol*. Jan 2013;239:1-12.
7. Logan GD, Cowan WB, Davis KA. On the ability to inhibit simple and choice reaction time responses: a model and a method. *J Exp Psychol Hum Percept Perform*. Apr 1984;10(2):276-291.
8. Brown P, Oliviero A, Mazzone P, Insola A, Tonali P, Di Lazzaro V. Dopamine dependency of oscillations between subthalamic nucleus and pallidum in Parkinson's disease. *J Neurosci*. Feb 1 2001;21(3):1033-1038.
9. Jenkinson N, Brown P. New insights into the relationship between dopamine, beta oscillations and motor function. *Trends Neurosci*. Dec 2011;34(12):611-618.
10. Kuhn AA, Tsui A, Aziz T, et al. Pathological synchronisation in the subthalamic nucleus of patients with Parkinson's disease relates to both bradykinesia and rigidity. *Exp Neurol*. Feb 2009;215(2):380-387.
11. Wingeier B, Tchong T, Koop MM, Hill BC, Heit G, Bronte-Stewart HM. Intra-operative STN DBS attenuates the prominent beta rhythm in the STN in Parkinson's disease. *Exp Neurol*. Jan 2006;197(1):244-251.
12. Bronte-Stewart H, Barberini C, Koop MM, Hill BC, Henderson JM, Wingeier B. The STN beta-band profile in Parkinson's disease is stationary and shows prolonged attenuation after deep brain stimulation. *Exp Neurol*. Jan 2009;215(1):20-28.
13. Whitmer D, de Solages C, Hill B, Yu H, Henderson JM, Bronte-Stewart H. High frequency deep brain stimulation attenuates subthalamic and cortical rhythms in Parkinson's disease. *Front Hum Neurosci*. 2012;6:155.
14. Patil PG, Conrad EC, Aldridge JW, Chenevert TL, Chou KL. The anatomical and electrophysiological subthalamic nucleus visualized by 3-T magnetic resonance imaging. *Neurosurgery*. Dec 2012;71(6):1089-1095; discussion 1095.
15. Leventhal DK, Gage GJ, Schmidt R, Pettibone JR, Case AC, Berke JD. Basal ganglia beta oscillations accompany cue utilization. *Neuron*. Feb 9 2012;73(3):523-536.
16. Klostermann F, Nikulin VV, Kuhn AA, et al. Task-related differential dynamics of EEG alpha- and beta-band synchronization in cortico-basal motor structures. *Eur J Neurosci*. Mar 2007;25(5):1604-1615.

17. Ballanger B, van Eimeren T, Moro E, et al. Stimulation of the subthalamic nucleus and impulsivity: release your horses. *Ann Neurol*. Dec 2009;66(6):817-824.
18. Eagle DM, Baunez C. Is there an inhibitory-response-control system in the rat? Evidence from anatomical and pharmacological studies of behavioral inhibition. *Neurosci Biobehav Rev*. Jan 2010;34(1):50-72.
19. Obeso I, Wilkinson L, Jahanshahi M. Levodopa medication does not influence motor inhibition or conflict resolution in a conditional stop-signal task in Parkinson's disease. *Exp Brain Res*. Sep 2011;213(4):435-445.
20. Ray NJ, Jenkinson N, Brittain J, et al. The role of the subthalamic nucleus in response inhibition: evidence from deep brain stimulation for Parkinson's disease. *Neuropsychologia*. Nov 2009;47(13):2828-2834.
21. Lopez-Azcarate J, Tainta M, Rodriguez-Oroz MC, et al. Coupling between beta and high-frequency activity in the human subthalamic nucleus may be a pathophysiological mechanism in Parkinson's disease. *J Neurosci*. May 12 2010;30(19):6667-6677.
22. Alegre M, Alvarez-Gerriko I, Valencia M, Iriarte J, Artieda J. Oscillatory changes related to the forced termination of a movement. *Clin Neurophysiol*. Feb 2008;119(2):290-300.
23. Ray NJ, Brittain JS, Holland P, et al. The role of the subthalamic nucleus in response inhibition: evidence from local field potential recordings in the human subthalamic nucleus. *Neuroimage*. Mar 2012;60(1):271-278.
24. Swann N, Poizner H, Houser M, et al. Deep brain stimulation of the subthalamic nucleus alters the cortical profile of response inhibition in the beta frequency band: a scalp EEG study in Parkinson's disease. *J Neurosci*. Apr 13 2011;31(15):5721-5729.
25. Picton TW, Stuss DT, Alexander MP, Shallice T, Binns MA, Gillingham S. Effects of focal frontal lesions on response inhibition. *Cereb Cortex*. Apr 2007;17(4):826-838.
26. Serrien DJ, Orth M, Evans AH, Lees AJ, Brown P. Motor inhibition in patients with Gilles de la Tourette syndrome: functional activation patterns as revealed by EEG coherence. *Brain*. Jan 2005;128(Pt 1):116-125.

Chapter 6 : Conclusion

The presented work demonstrates a substantial validation of the development of an intraoperative data acquisition system for use in deep brain stimulation surgery. This system is of considerable use for both research and clinical applications. IODA has been shown to improve clinical targeting of the STN using MR images and analyzed electrophysiological signals. IODA has also enabled the structural mapping of the STN using local field potentials to properly identify optimal sites for chronic stimulation for the treatment of Parkinson disease. Additionally it was demonstrated that integration of experimental tasks for use intraoperatively was possible to confirm recent findings regarding the physiological role of the STN in movement control. The development and subsequent broad validation of this system has enabled significant research to be possible during DBS surgery. It has also proven to offer neurosurgeons with a wide range of experience to participate confidently and safely in brain stimulation procedures.

This system is capable of being applied in other DBS surgical procedures and brain surgeries. There is potential for IODA to be incorporated into DBS for Essential Tremor with stimulation in the ventrointermediate nucleus (VIM). Both for clinical and research applications, IODA can potentially enable improved targeting of the VIM through the use of broadband MER signals and high resolution imaging. There is significant impact on patient quality of care and DBS device longevity with research into alternative chronic stimulation parameters. Until now, customizable stimulation parameters were not available and the possibility to explore stimulation with improved outcomes and reduced energy consumption was lacking. IODA also has the potential to be applied into other types of clinical brain surgeries requiring precise localization. These surgeries include tumor excisions, DBS for depression, epileptic surgery, pallidotomy, and thalamotomy.

A novel and highly adaptable intraoperative neural stimulation and recording system is presented here with significant impact to research and clinical applications of deep brain stimulation.

Appendix

IODA USER MANUAL

version EVERLAST_20130320

Sunjay Dodani & Charles Lu

Contents

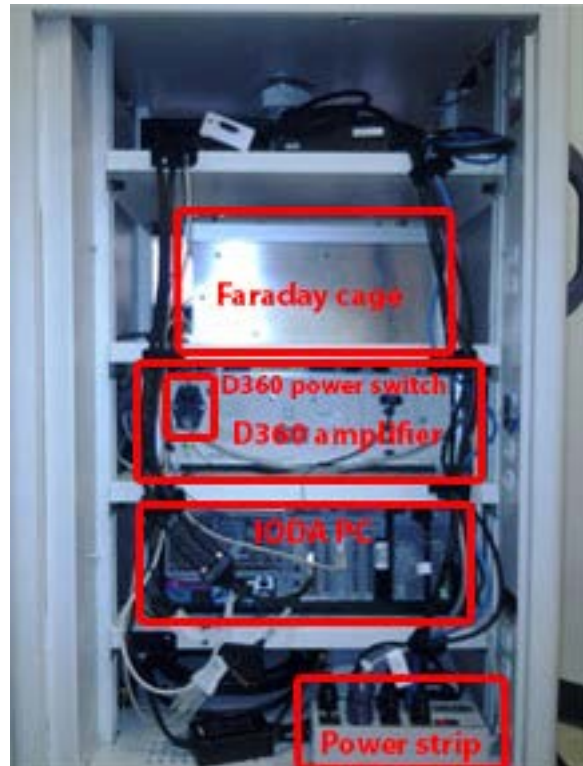
HARDWARE SETUP INSTRUCTIONS	69
SOFTWARE INITIALIZATION	72
CONNECTING TO THE PATIENT.....	76
INTRAOPERATIVE MONITORING AND RECORDING	77
MRI OBSERVATION IN NEUROSUITE	78
CONTROLLING PROBE DEPTH.....	79
STIMULATION.....	81
SYSTEM TEARDOWN	83
KNOWN ISSUES AND TROUBLESHOOTING.....	85

Hardware Setup Instructions

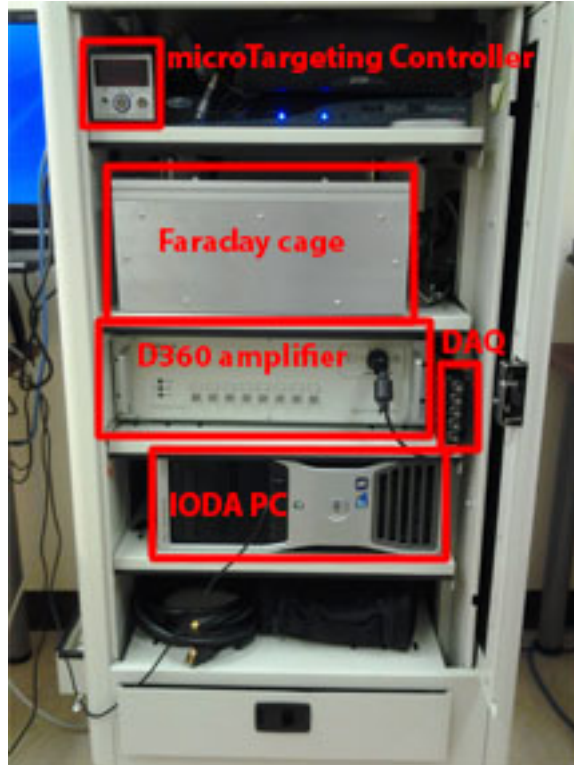
1. Power the IODA rig:
 - a. Plug in the white power cord on the outside of the IODA rig.
 - b. Open the back cover of the IODA rig and turn on the power strip at the bottom.
 - c. Turn on the D360 amplifier.
 - d. Close the back cover.



Side of the IODA rig.



Back side of the IODA rig.



Front side of the IODA rig.

2. Connect IODA to external hardware. On the front side of the IODA rig:

- a. Connect the microTargeting remote control to the microTargeting Controller unit. Locate the motor, but do not connect it to the Controller. The motor will be connected in a later step.
- b. Turn on the IODA PC and plug in the mouse and keyboard (stored beneath the PC) into the two front USB jacks.
- c. The IODA rig has two external DVI outputs above the white power cable. Using the DVI cable stored beneath the PC, connect the top DVI output to the nearest wall-mounted external display.
- d. Turn on the monitor mounted on the top of the IODA rig and reorient to face the front of the IODA rig.



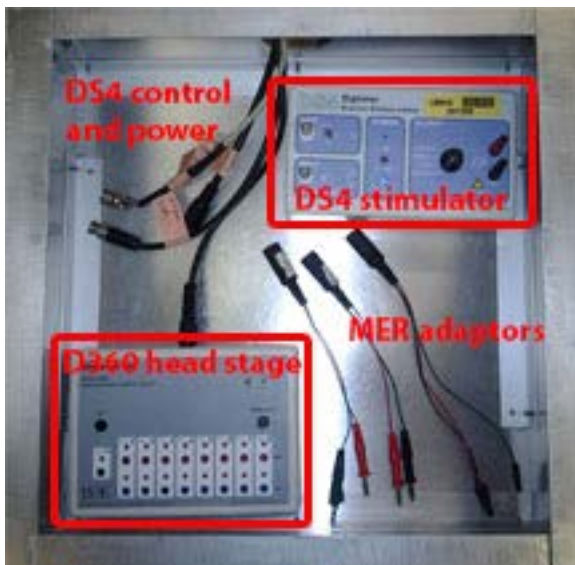
microTargeting remote control

- e. Using the oval remote found near the MTC, click buttons 1 and 14, pointing the remote at the 4x4DVIDLMatrix next to the MTC.
Note: If the DVI cable is connected to the lower output, click buttons 2 and 13 on the DVIDLMatrix instead.



Oval DVIDLMatrix remote.

3. Set up the Faraday cage:
 - a. Carefully pull the Faraday cage from the IODA rig and place on a non-conducting surface. *Note: A blanket, stored beneath the PC, can be placed under the cage to insulate it from a conducting surface.*
 - b. Orient the unused opening of the Faraday cage toward the patient.
 - c. Check that the RECORD adaptor is plugged into Input 1 of the D360 head stage, with the green connector in the COM jack, the red connector in the blue jack, and the black connector in the red jack.



Inside of the IODA Faraday cage.

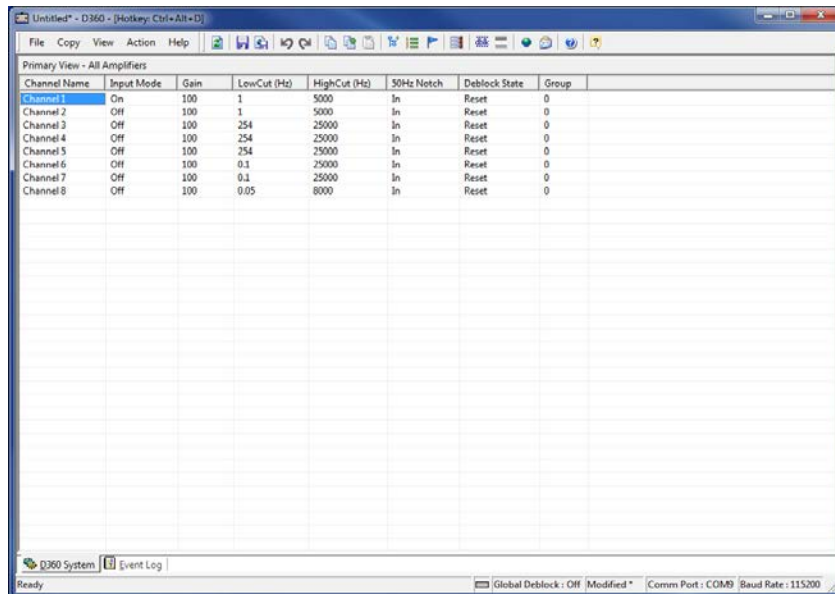


The D360 amplifier head stage.

Software Initialization

1. Log onto the IODA PC.
2. Check PC volume, adjusting volume through Windows or speaker volume knob as needed. Volume should be clearly audible to the surgeon. *Note: the PC speaker is located next to the microTargeting Controller unit.*
3. Navigate to C:\Users\IODA\Desktop\OR SOFTWARE .
4. Open the D360 client.
5. Open the IODA GUI. *Note: opening the IODA GUI will also open Neurosuite and the ET patient interface.*

D360 client initialization



The screenshot shows a window titled "Unlabeled - D360 - [Hotkey: Ctrl+Alt+D]". The window contains a table with the following data:

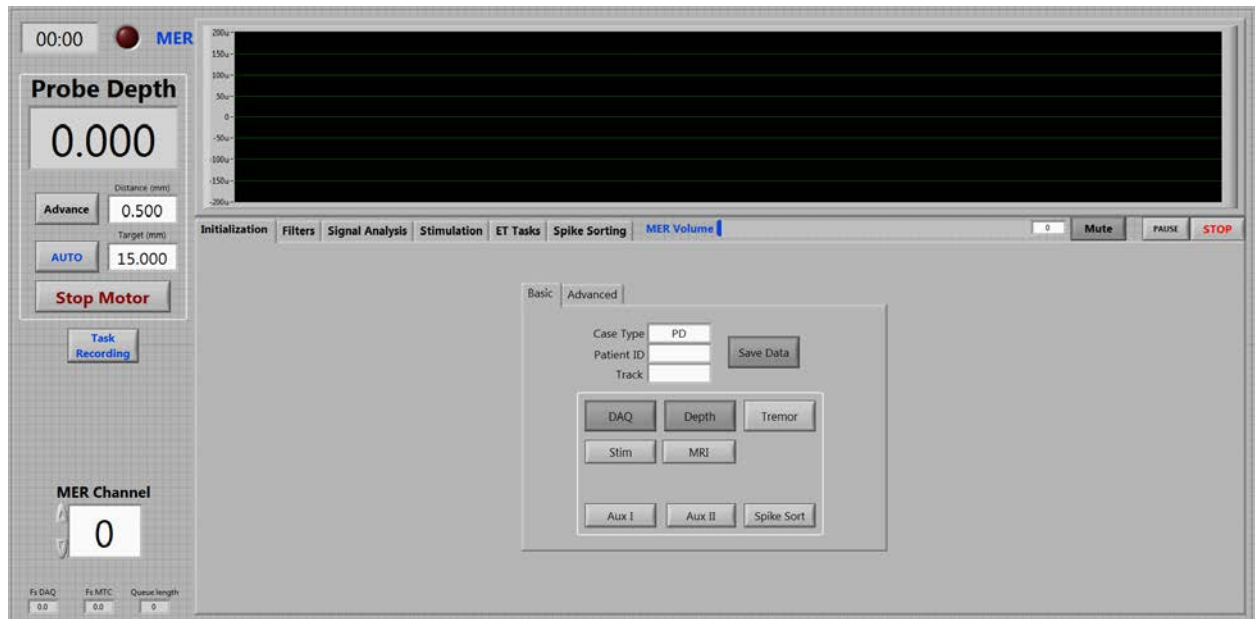
Channel Name	Input Mode	Gain	LowCut (Hz)	HighCut (Hz)	50Hz Notch	Deblock State	Group
Channel1	On	100	1	5000	In	Reset	0
Channel2	Off	100	1	5000	In	Reset	0
Channel3	Off	100	254	25000	In	Reset	0
Channel4	Off	100	254	25000	In	Reset	0
Channel5	Off	100	254	25000	In	Reset	0
Channel6	Off	100	0.1	25000	In	Reset	0
Channel7	Off	100	0.1	25000	In	Reset	0
Channel8	Off	100	0.05	8000	In	Reset	0

The window also shows a status bar at the bottom with the following information: "D360 System", "Event Log", "Ready", "Global Deblock: Off (Modified)", "Comm Port: COM3", and "Baud Rate: 115200".

Note: These steps must be performed *after* turning on the D360 amplifier system.

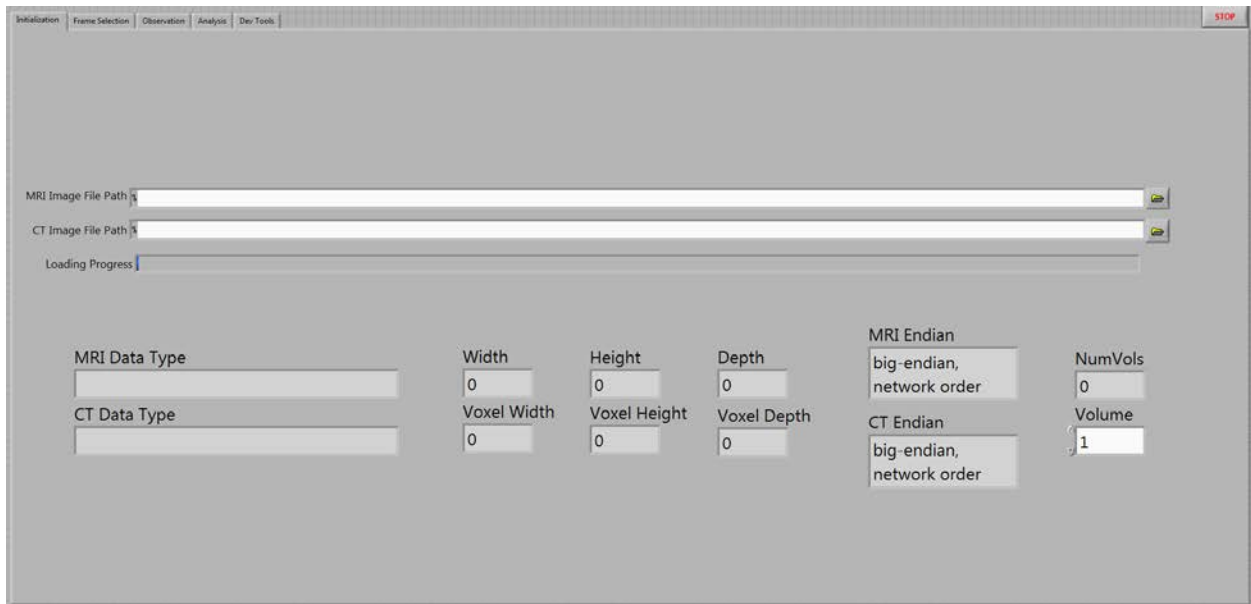
1. Change window focus to the D360 client.
2. Check that all eight inputs are displayed as shown above.
 - a. Initialization of settings is automatic.
Note: no items will be shown in the window if initialization fails. If initialization fails, check that the D360 is powered on and the head stage is plugged in, then close and reopen the D360 client.
3. Minimize the window.
 - a. The D360 client will minimize to the system tray rather than the taskbar.

EVERLAST initialization

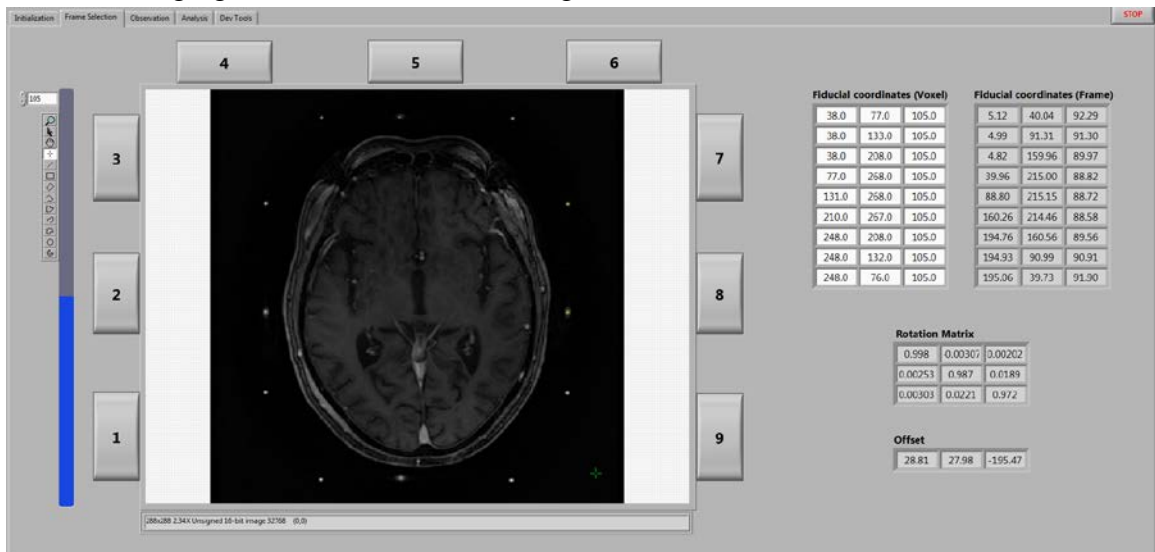


1. By default, the IODA GUI opens to the **Initialization** tab. If the Initialization tab is not selected, navigate to it by clicking on its tab.
2. Select the **Case Type** and enter the **Patient ID** and **Track**.
 - a. **Case Type** options: STN (Parkinson's disease), VIM (essential tremor), C25 (major depression), and Test
 - b. **Patient ID** is a combination of the patient's first and last initials and the last four digits of their UMHS ID. *Example: for patient John Smith, UMHS ID 987654321, enter JS4321.*
 - c. **Track** indicates the side (RT or LT) and attempt number on each side. *Examples: LT1 for the first left-side track, RT2 for the second right-side track.*
3. Choose whether to **Save Data**. By default, **Save Data** is turned on.
4. Select the appropriate functionalities. By default, **DAQ** (for MER) and **Depth** (for MTC) are turned on.
 - a. For ET cases, turn on **Stim**.
 - b. When MRI data is available, turn on **MRI**.

Neurosuite initialization



1. By default, Neurosuite opens to the **Initialization** tab. If the **Initialization** tab is not selected, navigate to it by clicking on its tab.
2. Click on the folder icons to the right of the **MRI Image** and **CT Image File Path** fields to browse to the appropriate imaging files.
 - a. Image files will be provided by the neurosurgeon on a USB flash drive.
 - b. MRI image files will typically be denoted by a “3TC” in the file name.
3. Hit CTRL+R to run the Neurosuite module.
4. Once the imaging files have finished loading, switch to the **Frame Selection** tab.



Note: if no image has appeared after files have completed loading, right click on the images and select Zoom to Fit.

5. Using the blue slider bar, select to an appropriate transverse slice on which to select fiducial coordinates. *Note: the slice with the longest AC-PC line is typically used.*
6. Using the crosshair tool (shown right) to the left of the slider bar, select fiducial #1 (bottom of the right side). Then click on the **1** button adjacent to the image.
7. Proceed clockwise around the image, selecting fiducials with the crosshair and clicking on the corresponding number button until all nine fiducials have been selected. (The bottom three are unused.)

Note: The magnifying glass tool, also found on the tool strip shown right, can be used to better pinpoint fiducial coordinates. Dragging the crosshair near the edges of the image scrolls the image when zoomed in.

8. Once all fiducials have been selected, hit the STOP button to stop the VI. All fiducial coordinates will be saved as long as Neurosuite remains open.

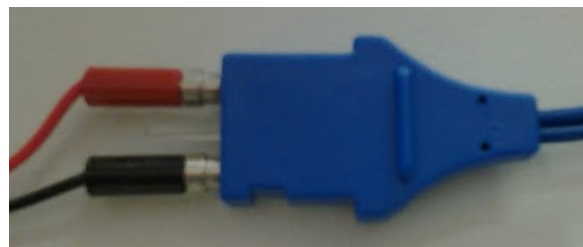


Connecting to the Patient

1. Connect to the patient:
 - a. Attach the REM Polyhesive Adult Patient Return Electrode (usually connected to the Bovie) to the red male connector in the Faraday cage.
 - b. When the neurosurgeon presents the MER signal cable, connect it to the RECORD adaptor attached to the D360 head stage.
2. Connect the microTargeting motor:
 - a. When the neurosurgeon presents a plastic sheath, remove the microTargeting motor's cap and place the motor in the plastic sheath.
 - b. Extend the sheath and attach the adhesive end to the side of the IODA rig.
 - c. Plug the microTargeting motor into the microTargeting Controller.
 - d. Turn on the microTargeting Controller by flipping the switch on the back of the unit (near the top of the unit).
 - e. Click the button on the front of the microTargeting Controller to zero the unit.
Note: Do not click the button again after zeroing the Controller.
3. Replace the lid on the Faraday cage.



microTargeting motor



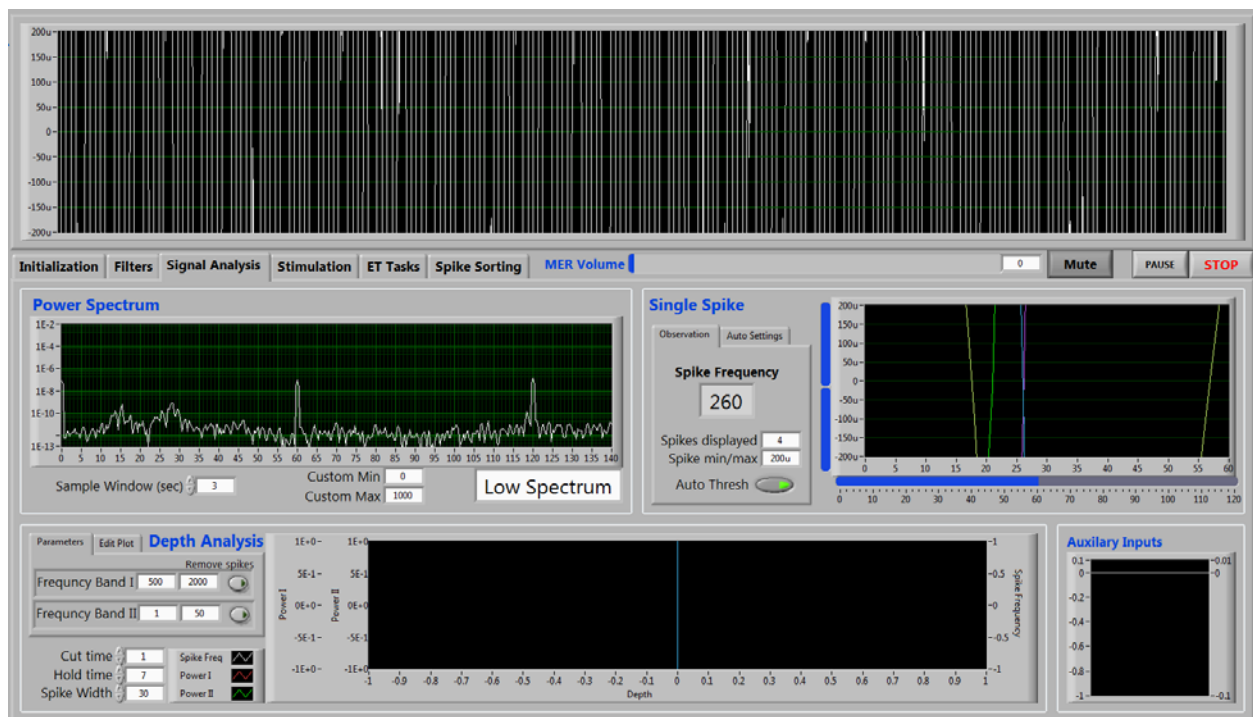
REM Polyhesive Adult Patient Return Electrode connector (right) and red and black male connectors in the Faraday cage (left).

Intraoperative Monitoring and Recording

After setup and initialization are complete, bring the IODA GUI window into focus and hit CTRL+R to begin recording. Intraoperative monitoring can be performed on the **Signal Analysis** tab.

Initialization checklist:

- The D360 amplifier system is turned on and the D360 client software was initialized *after* turning on the hardware unit.
- The microTargeting Controller is turned on and zeroed, with motor and remote control plugged in.
- The REM Polyhesive Adult Patient Return Electrode is connected in the Faraday cage.
- Patient name and ID, case type, and track are entered in the IODA GUI.



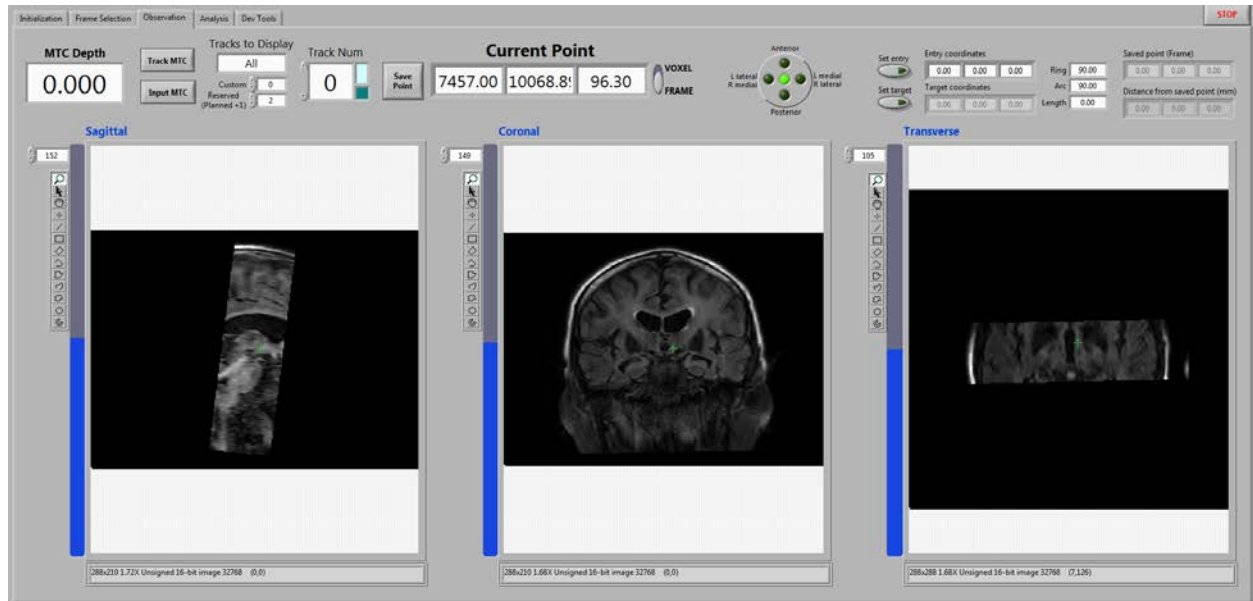
At the top of the IODA GUI is the primary signal display. The filtered, gain-removed microelectrode recording is shown here. Filter settings can be adjusted in the **Filters** tab.

Beneath the primary signal display are the Volume Slider, **Mute** button, Pause button, and **STOP** button. The **STOP** button performs a soft stop of the VI when pressed and held down. If this button fails to completely stop the VI, use the hard stop afterwards with CTRL+period.

Note that volume is MUTED by default. See Known Issues to address signal saturation.

MRI Observation in Neurosuite

Note: Neurosuite will automatically run if MRI is turned on during initialization.



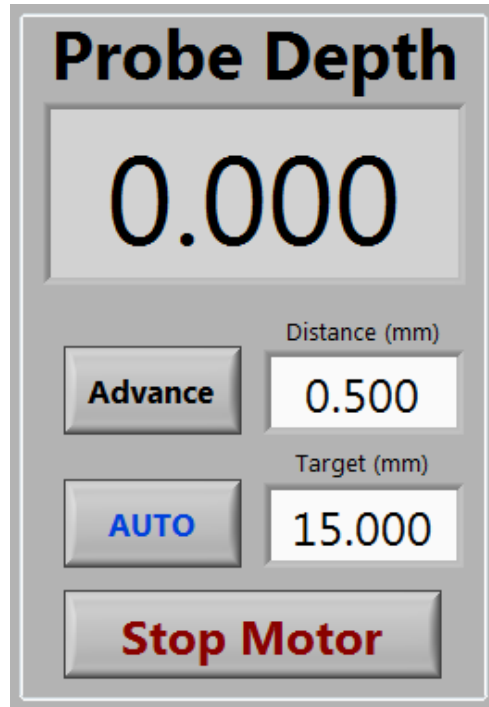
MRI observation can be performed on the Observation tab in Neurosuite.

Note: if no images have appeared after files have completed loading, right click on the images and select Zoom to Fit.

1. Enter target frame coordinates *and then* the ring, arc, and length in the appropriate fields at the top right of GUI (above the transverse image). *Note: Entry coordinates are automatically calculated from the above parameters.*
2. The crosshair tool and blue slider bars can be used to select slices to view. The crosshair indicates the same voxel in all three views. The magnifying glass tool can be used to zoom in on images.
3. Turn on Track MTC to track the probe along its track. *Note: when Track MTC is turned on, slices can no longer be manually selected for viewing.*
4. Neurosuite will stop automatically when the IODA GUI is stopped.

Controlling Probe Depth

Note: the following features will only function if Depth was turned on during initialization.



Probe Depth controls and displays are found near the top right corner of the IODA GUI.

1. To Advance:
 - a. Enter a step distance in the **Distance (mm)** field.
 - b. Hit **Advance** to advance the motor.
 - c. Hit **Stop Motor** to stop the motor at any time.

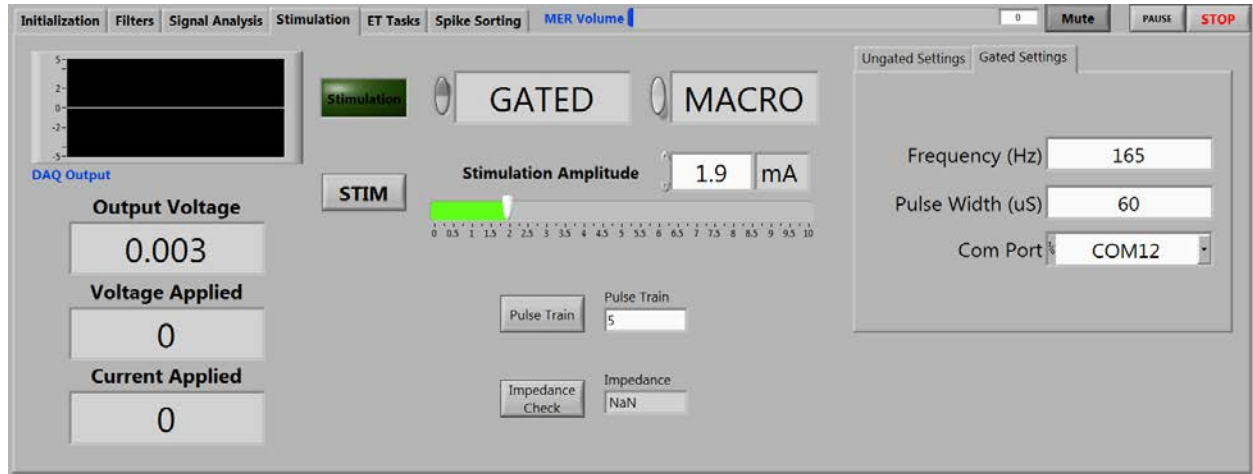
2. To Auto Advance:
 - a. Enter a step distance in the **Distance (mm)** field.
 - b. Enter a target depth in the **Target (mm)** field.
 - c. Turn on **AUTO**.
 - d. Hit **Advance** to begin advancing the motor.
 - e. Hit **Stop Motor** to stop the motor at any time.

3. To move backwards:
 - a. Use the physical microTargeting remote control. The software cannot move the probe backwards.

Note that the microTargeting remote control can also be used to control probe depth when not using the software's Advance command. See Known Issues to address "runaway" probe movement.

Stimulation

Note: the following features will only function if Stim was selected during initialization.



Stimulation controls and displays are found on the **Stimulation** tab. The DS4 stimulator unit is found inside the Faraday cage.



1. Prior to stimulation, hit the **Mute** button to mute MER signals.
2. Turn on the DS4.

3. Turn on the Gate switch on the DS4.
4. Select between macro and microstimulation:
 - a. To apply MACROSTIMULATION:
 - i. Plug the macrostim adaptor to the DS4 output. Plug the green connector to the black output of the DS4 and the red connector to the red output of the DS4.
 - ii. Select 10mA on the DS4 Output dial.
 - iii. Select the **MACRO** option on the **Stimulation** tab.
 - b. To apply MICROSTIMULATION:
 - i. Plug the microstim adaptor to the DS4 output. Plug the black connector to the red output of the DS4 and the red connector to the black output of the DS4.
 - ii. Select 100 μ A on the DS4 Output dial.
 - iii. Select the **MICRO** option on the **Stimulation** tab.
5. Disconnect the MER cable from the D360 amplifier and connect the MER cable to the adaptor.
6. Select between gated and ungated stimulation:

Note: the gate switch on the DS4 should be ON for both gated and ungated stimulation.

 - a. To apply GATED stimulation:
 - i. Plug the Gate Signal cable to the DS4 Gate input.
 - ii. Select the **GATED** option on the **Stimulation** tab.
 - iii. Check settings in the **Gated Settings** tab (within the **Stimulation** tab).
Note: only square waves can be output with gated stimulation.
 - b. To apply UNGATED stimulation:
 - i. Unplug the Gate Signal cable from the DS4 Gate input.
 - ii. Select the **UNGATED** option on the **Stimulation** tab.
 - iii. Check settings in the **Ungated Settings** tab (within the **Stimulation** tab.)
7. Apply stimulation:
 - a. Select the **Stimulation Amplitude** using the slider or by entering a value into the digital display.
 - b. Click **STIM** to apply stimulation. Click again to stop stimulation. **Pulse train** can be used to apply stimulation for a preset period.
Note: A green Stimulation icon will light up and an audio tone will play when stimulation is being applied.

System Teardown

After DBS probe placement is confirmed, the IODA system can be powered down, disassembled, and returned to the research laboratory.

1. Shut down the IODA PC:
 - a. Check that the IODA interface has been stopped.
 - b. Shut down the IODA PC.
 - c. Detach keyboard and mouse.
 - d. Store keyboard and mouse underneath IODA PC.
 - e. Detach DVI cable from external display and external output.
 - f. Coil DVI cable and store underneath IODA PC.
 - g. Reattach original DVI cable to external display.

2. Store the Faraday cage:
 - a. Detach the MER signal cable from adaptors in the Faraday cage and remove from the Faraday cage.
 - b. Detach the Red Cable from the D360 head stage, if used, and remove from the Faraday cage.
 - c. Turn off the DS4, if used.
 - d. Replace the lid on the Faraday cage.
 - e. Slide the Faraday cage into the empty shelf in the IODA rig. Orient the cage such that cables exit the Faraday cage on the right hand side.
 - f. Fold the blanket, if used, and store beneath the IODA PC.

3. Power down the IODA rig:
 - a. Shut off the microTargeting Controller with the switch on the back of the unit.
 - b. Shut off the D360 amplifier with the switch on the back of the unit.
 - c. Shut off the power strip, located behind the back panel of the IODA rig.
 - d. Unplug the IODA rig and store power cable on the rig's external handle.

4. Store the microTargeting Controller:
 - a. Unplug the microTargeting motor and remote control from the microTargeting Controller.
 - b. Store the microTargeting remote control next to the Controller unit.
 - c. Ask the surgeon to detach the microTargeting motor from the patient.
 - d. Remove the microTargeting controller from the plastic sheath.
Note: The use of gloves is recommended for this step, as the sheath and motor may have had contact with patient fluids.
 - e. Replace the cap on the microTargeting motor.
 - f. Store the microTargeting motor next to the Controller unit.

Known Issues and Troubleshooting

Runaway probe movement:

Failure to zero the microTargetting Controller prior to running the IODA VI will cause the motor to advance until the controller unit is shut off. The motor cannot be controlled using either the software controls or the physical remote control when this occurs. After shutting off the controller unit, the motor must be manually returned to its zero position before resuming.

Signal saturation:

Signal saturation is indicated by prolonged observation of low-amplitude noise ($\sim 25 \mu\text{V}$) with no movement artifact during motor movement. After hitting **MUTE** on the IODA interface:

1. Have the surgeon attach a sterilized Red Cable to the external cannula with the alligator clip end. Plug the other end into the blue input of the D360 head stage, in place of the MER adaptor's red connector. Check for signal restoration.
2. If Step 1 fails to restore signal, have the surgeon clip the Red Cable to the retractor on the patient. Check for signal restoration.
3. If Step 2 fails to restore signal, plug the black male connector in the Faraday cage into the REM Polyhesive Adult Patient Return Electrode connector. Check for signal restoration with the Red Cable clipped to the external cannula and to the retractor.